LUND UNIVERSITY

Master Thesis

Poly(*p*-terphenyl piperidinium) as anion exchange membranes. Synthesis and evaluation of properties

by

Hugo Selling

Centre for Analysis and Synthesis
Lund University
Sweden
August 26, 2020

Supervisor: **Professor Patric Jannasch**
Examiner: **Associate Professor Baozhong Zhang**

Postal address
PO-Box 124
SE-221 00 Lund, Sweden
Web address
www.kilu.lu.se/cas/

Visiting address
Naturvetarvägen 14

Telephone
+46-222 83 49

Lund 2020

Acknowledgements

This master thesis was performed at the Centre for analysis & Synthesis at Kemicentrum in Lund.

First and foremost i would like to thank my supervisors Dong Pan and Patric Jannasch. Thanks to Patric for giving me the opportunity to do my master thesis in a important and interesting subject. Thanks Dong for your patience when helping me in the lab, answering my questions and checking my NMR spectra, this would have been so much harder without you.

I would also like to thank all the people in the polymer group for all the help. Special Thanks to Joel Olsson for letting me borrow his fume hood and answering all sorts of questions. Thanks to Andrit Allushi for the help and reminding me when there is time for coffee. Thanks to Thanh Huong Pham for answering questions. Thanks to Hannes Nederstedt for reminding me than I'm a master student. Thanks Giorgia for the chats in the lab and the discussions about our master thesis work.

I would also thank my girlfriend and cat for helping and supporting me.

Thank You!

Abstract

Alkaline exchange membrane fuel cells (AEMFC) is an interesting and attractive alternative to proton exchange membrane fuel cells (PEMFC) due to the potential use of non-precious catalysts which can reduce the overall cost of the fuel cell. An important component of the AEMFC is the anion conducting membrane. This membrane needs to possess several important properties such as a high hydroxide conductivity and sufficient stability at elevated temperatures for a prolonged time. The membrane material is a polymer which structure affects the properties. Extensive research has been made in the last decade in order to find a material that posses all the required properties.

In this work, polymers with an all-carbon based backbone and incorporated piperidinium ions, poly(*p*-terphenyl piperidnium), are synthesized and studied with regards to the structure of the piperidinium ion. Two different polymers were synthesized *via* superacid catalyzed polycondensations of *p*-terphenyl, with either 4-piperidone or *N*-methyl-4-piperidone. These polymers were then functionalized *via* Menshutkin reactions with alkyl and benzylic halides of different sizes and structures. Seven polymers were successfully synthesized. Three more were attempted, but unsuccessful due to sterical restrictions in the functionalization step, e.g. a limit with regard to the size of the alkylhalide used. Three of the successfully synthesized polymers poly(*p*-terphenyl *N*-methyl-*N*-isobutyl-piperidinium), poly(*p*-terphenyl *N*-methyl-*N*-cyclohexylmethyl-piperidinium) and poly(*p*-terphenyl *N*-methyl-*N*-benzyl-piperidinium) were evaluated as hydroxide exchange membranes. The evaluated polymers displayed OH^- conductivities of over 100 mS cm^{-1} but poor alkaline stability and high water uptake. The properties that the evaluated polymers displayed related to the size and structure of the extender group.

Sammanfattning

Alkaliska bränsleceller är ett intressant och attraktivt alteranativ till dagens protonledande bränsleceller på grund av den potentialla användningen av billigare katalysatormaterial vilken kan leda till en minskad kostnad för bränslecellen.

En viktig komponent i dessa alkaliska bränsleceller är det anjonledande membranet. Detta membran behöver ha flera viktiga egenskaper såsom hög jonledningsförmåga och stabilitet vid höga temperaturer under lång tid. Membranmaterialet är en polymer vars struktur påverkar egenskaperna och omfattande forskning har gjorts under det senaste årtiondet för att hitta ett material som har alla de önskade egenskaperna.

I detta arbete har polymerer med en kolbaserad grundkedja och inkorporerade piperidniumjoner av olika strukturer, syntetiserats och studerats. Två olika polymerer syntetiserades *via* supersyra katalyserade polykondensationer mellan *p*-terphenyl och 4-piperidone eller *N*-methyl-4-piperidone. Dessa polymerer funktionaliserades sedan *via* Menshutkin reaktioner med alkyl- eller benzyl halider av varierande storlek och struktur. Detta resulterade i sju polymerer med varierande struktur på piperidiniumjonen. Ytterliggare tre polymerer försökte syntetiserats men på grund av steriska restriktioner i funktionaliseringssteget så var detta inte möjligt. Tre av de syntetiserade polymererna poly(*p*-terphenyl *N*-methyl-*N*-isobutyl-piperidinium), poly(*p*-terphenyl *N*-methyl-*N*-cyclohexylmethyl-piperidinium) och poly(*p*-terphenyl *N*- methyl-*N*-benzyl-piperidinium) utvärderades som hydroxidjonledande membran. De utvärderade polymererna hade alla en OH^- ledningsförmåga på över 100 mS cm^{-1} men dålig alkalisk stabilitet och ett högt vattenupptag. Egenskaperna som de utvärderade polymererna hade kunde förknipas med storleken och strukturen på förlängningsgruppen.

Populärvetenskaplig sammanfattning

En av de största utmaningarna världen står inför är omställningen från icke-förnyelsebara till förnyelsebara energikällor. Vissa av de förnyelsebara energikällorna, såsom vind- och solkraft har dock ett problem, nämligen att energin från dessa källor är svåra att lagra. När det blåser mycket eller solen lyser starkt produceras ibland mer energi (elektricitet) än vad som förbrukas, och då går denna elektricitet till spillo. När det däremot är vindstilla eller svag sol så produceras kanske mindre elektrictet än vad som behövs. Vi behöver därför komma på nya innovativa tekniska lösningar för att kunna lagra denna energi. En potential lösning är att omvandla den genererade elektriciteten från dessa energikällor till vätgas. Denna vätgas kan lagras för att sedan, när energin behövs, återigen omvandlas till elektricitet. Denna omvandling kan ske i en så kallad bränslecell.

En bränslecell är en elektrokemisk anordning, vilken kan liknas vid ett batteri. Bränslecellen omvandlar vätgas tillsammans med syre till elektricitet och vatten. Detta sker genom kemiska reaktioner i olika ändar av bränslecellen, precis som att det sker kemiska reaktioner vid plus och minuspolen i ett vanligt batteri. I dessa reaktioner bildas joner och elektroner, vilka båda är små laddade partiklar. Det är elektronerna som ger upphov till den elektriska strömmen, men för att kunna utvinna elektrictet behöver jonerna och elektronerna separeras i bränslecellen. Detta uppnås genom att en komponent i bränslecellen endast släpper igenom joner medan en annan endast släpper igenom elektronerna. Komponenten i bränslecellen som leder joner kallas elektrolyt. Beroende på vad för material elektrolyten är gjord av så kommer den att leda olika typer av joner. Detta i sin tur påverkar vilka reaktioner som sker i bränslecellen, vilket ytterligare leder till olika krav på materialen som bränslecellen är uppbyggd av. Kort och gott har materialen bränslecellen är uppbyggd av stor betydelse.

Bränsleceller har flera användningsområden men det mest välkända är nog bilar. I bilar används bränslecellen för att driva en elektrisk motor och det finns bränslecellsdrivna bilar redan idag. Bränslecellerna som används dessa bilar har dock problem, vilket bl.a. är deras pris. En av de största anledningarna till det höga priset är användandet av den sällsynta och dyra metallen platina. Användandet av platina ökar kostnaden för bränslecellen avsevärt. I dessa typer av bränsleceller är elek-

trolyten ett ett så kallat membran, som släpper igenom positivt laddade joner (protoner). Genom att byta ut membranet som leder protoner till ett membran som leder en annan sorts joner så kan man också byta ut platinat till något billigare.

Att byta ut membranet är inte speciellt lätt eftersom man då ändrar vilka reaktioner som sker men även vad för kemisk miljö som uppstår i bränslecellen. Membranen har flera krav på sig som behöver uppfyllas, såsom att jonerna lätt måste kunna ta sig igenom membranet. Membranet får inte heller gå sönder p.g.a. den temperatur eller miljö som råder i cellen. Allt detta påverkas av den molekylära strukturen på det material som membranet består av. Genom forskning försöker man komma på en molekylär struktur som uppfyller alla dessa krav.

I detta arbete tillverkades membran med olika molekylär struktur. Membranen undersöktes sedan för att se hur väl de uppfyllde de olika kraven och hur den molekylära strukturen påverkade de önskade egenskaperna. Detta arbete är viktigt för att i framtiden kunna utveckla bättre och billigare bränsleceller. Vi behöver kunna lagra och använda mer förnyelsebar energi som en del av ett mer hållbart och miljövänligt samhälle.

List of abbreviations

- IEM - Ion exchange membrane
- CEM - Cation exchange membrane
- AEM - Anion exchange membrane
- AEMFC - Anion exchange membrane fuel cell
- PEM - Proton exchange membrane
- PEMFC - Proton exchange membrane fuel cell
- IEC - Ion exchange capacity (meq. g^{-1} or mmol g^{-1})
- DIPEA - *N,N*-diisopropylethylamine
- NMP - *N*-Methyl-2-Pyrrolidone
- DMSO - Dimethylsulfoxide
- NMR - Nuclear magnetic resonance spectroscopy
- TGA - Thermogravimetric analysis
- DSC - Differential scanning calorimetry
- WU - Water uptake (%)

Contents

1 Introduction

In a world threatened by the climate crisis, a solution to the problem of using energy sources emitting carbon dioxide needs to be found. Renewable energy sources such as solar and wind are being developed all over the world since it may contribute to lower carbon emission. Some of these renewable energy sources have one major drawback though, which is their unreliability. The energy output from these sources cannot be controlled in the same way as traditional energy sources can which can lead to overproduction or underproduction of electricity. Developing an efficient way of storing and use energy from these renewable sources can solve this problem.

One of the potential ways of solving this is by using excess electricity to produce fuels, such as H_2 through electrolysis of water. This H_2 can then be stored and turned into electricity when needed with the help of a fuel cell. A fuel cell is a device which uses H_2 (or other fuels) in combination with oxygen to produce electricity. An important component of the fuel cell is the ion conducting membrane which is crucial in order for the fuel cell to work reliably and efficiently. Vehicles powered by fuel cells with proton conducting membranes exist today but are overshadowed by their battery driven counterparts. However, these fuel cells still have problems such as expensive materials needed to catalyze the reactions and expensive membrane material [20].

Replacing the proton conducting membrane with an alkaline exchange membrane (AEM) that conducts hydroxide ions has been suggested as a way to address some of these problems. Therefore, there has been an increasing interest in the last decade to develop these alkaline conducting membrane materials. Although, progress has been made these anionic conducting materials still have problems which have to be addressed if they are to compete with their proton conducting counterparts. These anionic conducting membrane materials consists of polymers with covalently linked cationic groups.

In this work alkaline conducting polymeric materials which is based on *p*-terphenyl with piperidinium cations have been synthesized and displays different properties

depending on the structure of the cation.

1.1 Aim

This works aims to see which extender groups can be used to quaternize poly(*p*-terphenyl piperidine) and how it affects the properties as an anion exchange membrane.

2 Background

Ion exchange membranes are used in a variety of different applications ranging from waste/wastewater treatment to electrodialysis. Several other applications are under development such as fuel cells, water electrolysers and redox flow batteris because of the need to convert and store renewable electricity. Ion exchange membranes consist of ionic head groups that are attached to a hydrophobic polymer backbone. They can be classified as anion exchange membranes (AEM) or cation exchange membranes (CEM) depending on the type of ion that can be permeate the membrane. An AEM has a positive head group attached to the polymer backbone while a CEM has negatively charged head group. See Figure 2.1 for a schematic image of a polymer used as AEM. The AEM lets anions permeate the membrane while keeping cations out and vice versa for a CEM. The AEM can be further classified by the conducted ions, if they let non-alkaline (e.g. Cl^- and SO_4^{2-}) or alkaline anions (e.g. OH^- and HCO_3^-) pass. The latter is called alkaline anion exchange membranes (AAEM) and these are being developed for the use in high-pH and high-temperature fuel cells (AEMFCs), and water electrolysis applications [6].

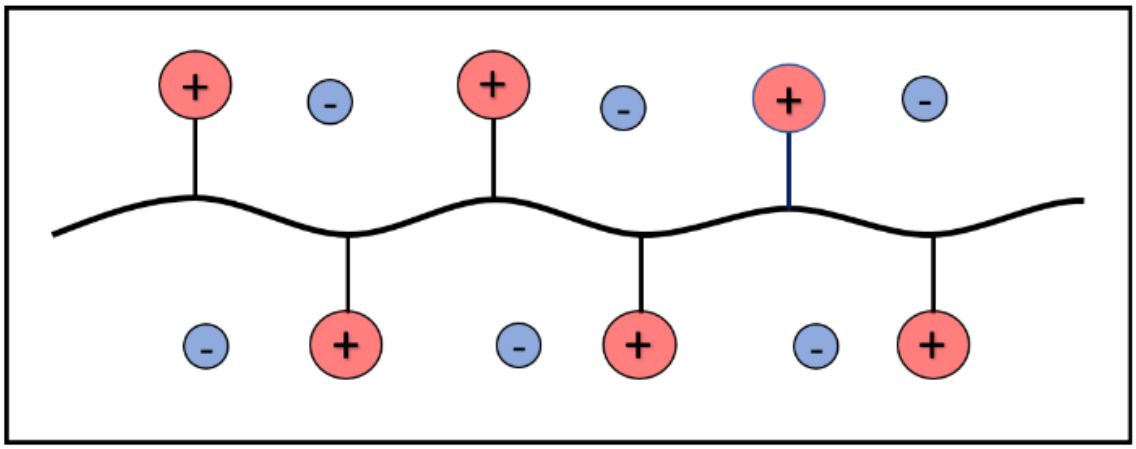

Figure 2.1 – Simple schematic of a cationic polymer

There are already today fully working fuel cells and other applications that use CEMs such as proton exchange membrane fuel cells (PEMFC) for vehicles, stationary applications [19] and proton exchange membrane water electrolysis [2]. The most common membrane material used in these type of applications is Nafion [7] and was developed in the 1960s by DuPont [17]. Although these PEM technologies work, they have drawbacks. This has caused a drive in research for the alkaline counterparts to get in line with these technologies.

The basic principles of how a fuel cell works, the difference between PEMFC and AEMFC, the requirements and current problems with OH^- conducting AEMs as well as structures of these materials and the effect it has on the properties will be discussed in the following parts.

2.1 Fuel cell working principles

The fuel cell is an electrochemical device that converts chemical energy stored in a fuel into electrical- and thermal energy. The fuel often mentioned is H_2, but other fuels, for example methanol, ethanol, ethylene glycol and methane can also be used. A simplified version of the fuel cell can be described as consisting of a cathode, an anode, an electrolyte (in our case the IEM) and electron conducting circuit [9].

The fuel is fed to the anode and oxygen is fed to the cathode. The fuel gets oxidized while the oxygen gets reduced. The electrons from the oxidized fuel pass through an external circuit while the ions generated pass through an electrolyte and water forms at one of the electrodes. This electrolyte is often what distinguishes different types of fuel cells and this electrolyte can either be a liquid or a solid [9].

To facilitate the oxidation and reduction reactions a catalyst needs to be used at both the anode and the cathode. The catalyst material used depends on fuel cell and type of fuel.

For the sake of simplicity, H_2 will be referred to as the fuel in this thesis.

2.2 AEMFC and PEMFC

The difference between AEMFCs and PEMFCs is the type of ion the electrolyte (membrane) conducts and the reactions which takes place at each electrode. In an AEMFC, H_2O, O_2 and electrons forms OH^- at the cathode which then passes through the electrolyte. At the anode H_2 gets oxidized and together with OH^- it forms H_2O and electrons. The generated electrons then pass through the external circuit to the cathode. The reactions are:

Cathode: $O_2 + 2\,H_2O + 4\,e^- \longrightarrow 4\,OH^-$

Anode: $H_2 + 2\,OH^- \longrightarrow 2\,H_2O + 2\,e^-$

Overall: $2\,H_2 + O_2 \longrightarrow 2\,H_2O$,

In a PEMFC H_2 gets oxidizied to H^+ and electrons at the anode, the protons is then conducted through the membrane to the cathode where they together with O_2 form water. The reactions are:

Cathode: $O_2 + 4\,H^+ + 4\,e^- \longrightarrow 2\,H_2O$

Anode: $2\,H_2 \longrightarrow 4\,H^+ + 4\,e^-$

Overall: $2\,H_2 + O_2 \longrightarrow 2\,H_2O$

Figure 2.2 shows simplified schematics of an AEMFC and PEMFC.

The overall reaction is the same, but the reactions taking place at the electrodes and the chemical environment in the cells are different. These different reactions and chemical environments leads to advantages and drawbacks for the two types of cells. The potential advantages regarding AEMFC in contrast to PEMFC are listed below and discussed to current status.

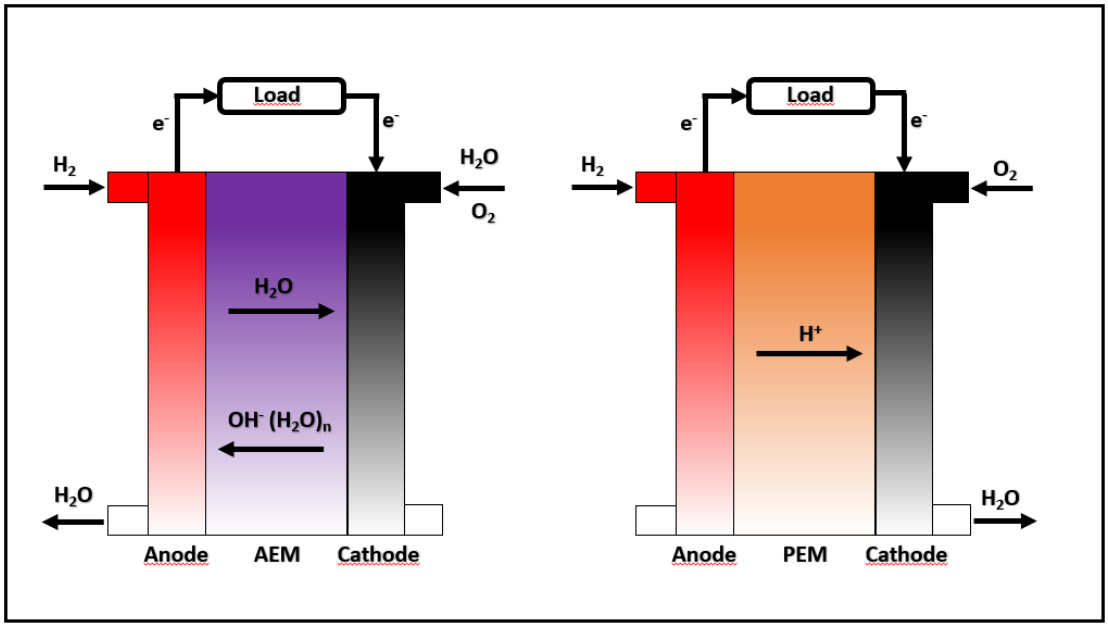

Figure 2.2 – Simplified schematic of an AEMFC (left) and a PEMFC (right)

2.2.1 Potential advantages of AEMFC compared to PEMFC

Some of the potential advantages of AEMFC compared to PEMFC is (1) cheaper catalyst material, (2) wider range of different cell and stack material, (3) a wider range of fuel.

1. *The use of non-platinum or non-precious metal-based catalysts.*
One drawback is that the PEMFC uses platinum as the catalyst material for both the anode and the cathode due to the acidic environment. This leads to an increased fuel cell cost and a potential limit on the availability of platinum might hinder commercialization [6]. The alkaline environment in an AEMFC also leads to faster reaction kinetics which potentially can lead for a reduction or removal of the need for the expensive Pt-based catalysts [18], this is primarily for the cathode oxygen reduction reaction [5]. The first alkaline fuel cells used a liquid electrolyte and AFC that use liquid electrolytes can operate using nickel/nickel-metal alloys and silver electrocatalyst [1]. The best performing AEMFCs still uses Pt based catalysts for both the anode and the cathode. However, cells that use Pt-free catalysts both in the anode and cathode have proven to work but these have a lower performance than their Pt-based counterparts [3]. The use of non-platinum or non-precious metal-based catalysts is often listed as the main reason for the drive to develop AEM.

2. *A wider range of different cell and stack materials which are stable in alkaline environment* [3].
The corrosion problems present in PEMFCs can be minimized in an alkaline environment [18].

3. *Ability to use a wider variety of fuels.*
In addition to the previously mentioned fuels, iso-propanol, sodium borohydride and nitrogen based fuels such as hydrazine or ammonia can be used in the AEMFC. The use of nitrogen based fuels in PEMFCs can lead to decrease in the fuel cell performance even at very low concentrations of ammonia (1 ppm).

2.2.2 Current issues and potential drawbacks with AEMFC

Some of the potential problems and drawbacks with using AEMFC is often related to (1) low OH^- conductivity, (2) carbonation, (3) water management, (4) alkaline stability.

1. *OH^- Conductivity and water uptake*
The diffusion coefficient of OH^- ion is about 4 times lower than that of the H^+ ion [18]. AEMs are therefore believed to need a higher ion exchange capacity (IEC), i.e. the AEMs needs to have a higher concentration of charged groups per gram of membrane material, in order to reach the same ionic conductivity as their PEM counterparts. In addition, IEC affects the amount of water that can be absorbed by the material. A too high IEC can lead to swelling of the membrane material due to excessive water uptake that can result in a loss of mechanical properties and loss of contact between the electrode and membrane layer. The water uptake is not only governed by the IEC but also by the visco-elastic forces holding the polymeric membrane together (which counteracts the osmotic pressure). This force can be increased by increasing the entanglement of polymer chains, or by cross-linking [11]. The morphology of the membrane is also important for the conductivity of the material and even though an excessive water uptake might ruin the membrane a certain amount of condensed water is needed within the membrane in order to form percolated pathways which helps with dissociation of the anion from the cationic groups [1, 18]. Phase separation between hydrophobic parts and interconnected ion rich clusters have been shown to increase conductivity at a lower water uptake. This

shows the importance of the architecture of the polymer structure [15].

The ionic conductivity of membranes are often given in milli Siemens cm^{-1} (mS cm^{-1}) and a higher value means a higher conductivity. Early AEM's rarely reached hydroxide ion conductivity's over 10 mS cm−1. The first AEM to reach over 100 mS cm^{-1} was produced by Coates and co-workers, however, the high IEC of their material resulted in 225 % water uptake at room temperature. Today a OH^- conductivity over 100 mS cm−1 is not rare [1] but comparing conductivity between different materials is difficult due to the difference and complexity in measuring conductivity [14].

2. *Carbonation*
An issue with the AEMFCs is their sensitivity to CO_2. OH^- in the membrane reacts easily with CO_2 forming carbonate species. This carbonate poisoning leads to a reduced performance of the AEMFC. The effects are not yet fully understood [14] but one reason might be due to the large carbonate ion having conductivity four to five times lower than that of the OH^- ion [6]. In laboratory scale measurements strategies to overcome this problem have been to use CO_2 free air, pure oxygen, degassed water and glove boxes with ultra-low CO_2 levels [6, 14]. Strategies for solving this problem on operational level include working at high current densities and therefore purge cell of carbonate species. Models have shown that working the fuel cell above 1 A cm^{-2} can reduce the amount of carbonate species present in the AEM [22]. Other strategies include operating at a temperature of 80 °C or greater to minimize the solubility of CO_2 in water based on Henrys law or outfitting the fuel cell with a regenerative filter which has been tested and reduced the level of CO_2 [1].

3. *Water management*
In PEMFCs water is produced at the cathode while in the AEMFC water is consumed and the cathode and formed at the anode. This leads to a special case where both water and OH^- needs to be transported across the membrane in opposite directions and the concentration of water in the different parts of the fuel cell can change during operation. The water is transported through two different mechanisms, self diffusion and electro-osmosis and these work in opposite direction in the AEMFC which leads to a more complex water management situation. The effect of a low

water content leads to low solvation of the OH^- ion which reduces the shielding effect that the water molecules have on the OH^- ion. This is believed to play a role in the stability of the membrane material [4].

4. *Alkaline stability*
A major issue in the development of stable and long-term working AEMFC is the chemical stability of the membrane/ionomer material in the highly alkaline and highly elevated temperature conditions in an AEMFC. The degradation can take place in the backbone where it can reduce the mechanical properties, and therefore, increase resistance or cause catastrophic failure. The degradation can also take place in the cationic groups which reduces the ionic conductivity and therefore increases the resistance. In addition to this the degradation can take place in the polymer-cationic group linkages [5]. The mechanisms and causes for the degradation will be discussed in section 2.3 regarding the structure of the polymeric material.

2.2.3 Requirements and important parameters

A technical target provided by the US department of energy states that in order for a single-cell AEMFC to be viable it needs to operate above 60°C at a current density of 600 mA/cm2 for 2000 hours with less than 10% voltage degradation. The membrane exchange assembly (MEA) with the highest power density could work at 600 mA/cm2 for 545 hours and had a 17 % voltage degradation [21].

To summarize the requirements of the polymeric membrane material for the use in AEMFCs, it needs to have: **High OH^- conductivity, optimal water uptake, alkaline stability, and mechanical and thermal stability**

2.3 Polymer structure

As mentioned earlier the polymeric material that the membrane consists of is made up by two different parts. The cationic moieties (or groups) that conducts the OH^- ions and the backbone to which the cationic groups are attached to which effect the mechanical properties of the membrane [21]. The stability of both these parts are important for the membranes overall stability. Different cations and backbones with regards to their stability will be discussed below.

2.3.1 Polymer backbone

Several different backbone structures have been explored such as polysulfones (PSU), poly(arylene ether ketones) (PAEK), poly(phenylene oxides) (PPO), polystyrenes (PS), polynorbornenes, polybenzimidazoliums (PBI), polyphenylenes polypropylenes (PP) and polyethylenes (PE) (Figure 2.3).

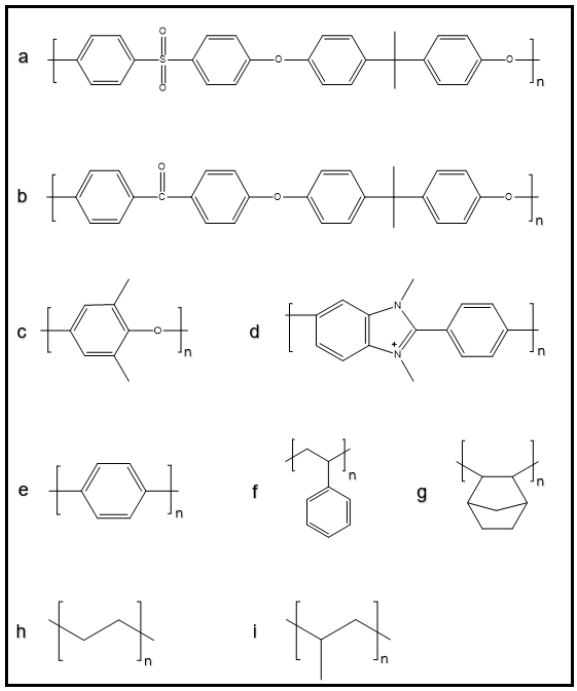

Figure 2.3 – Different polymer backbones employed in AEMs. a: PSU, b: PAEK, c: PPO, d: PBI, e: Poly(phenylene), f: PS, g: Poly(norbornene), h: PE, f: PP Adapated from ref [21] and [13]

Polymer backbones containing aryl ether bonds, see a-c in Figure 2.3, have been shown to be unstable due to cleavage of these bonds. It has been proposed that the cleavage is *via* nucleophilic aromatic substitution (SnAr) of the hydroxide anion when strong electron withdrawing groups, e.g. QA, is at the ortho position of the bond (Figure 2.4. It has been suggested that all carbon based polymer backbones are the most alkaline resilient and suitable for the use in AEM [13].

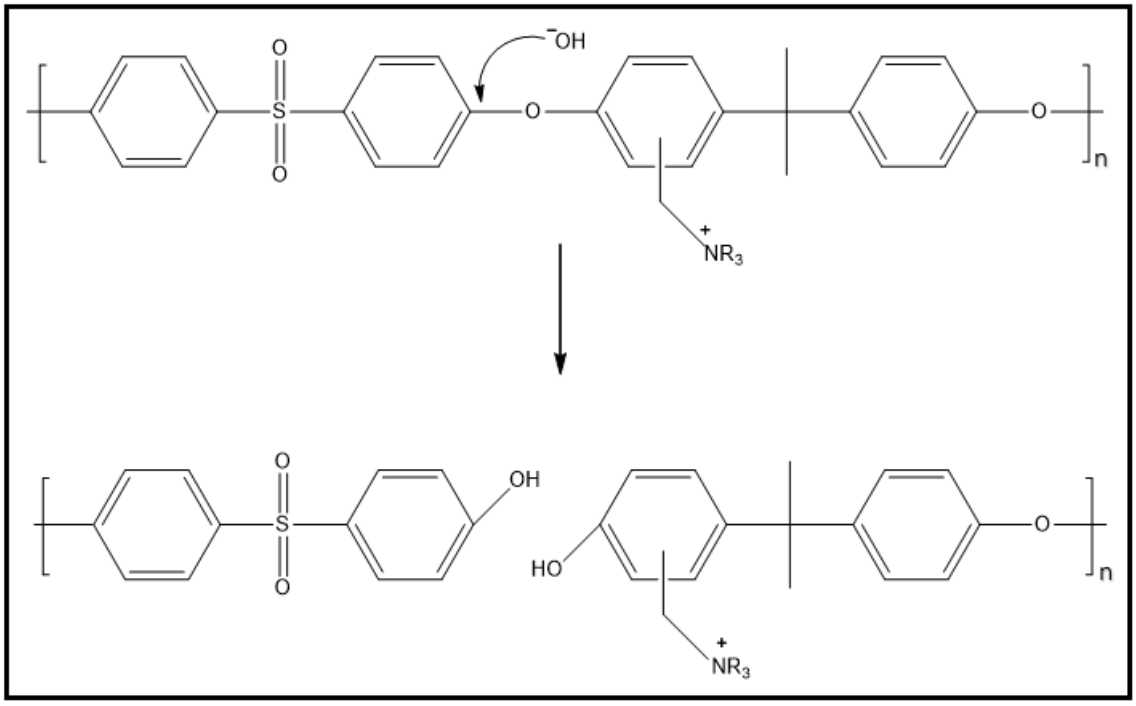

Figure 2.4 – Ether bond cleavage in PSU functionalized with QA. Adapted from ref [11]

2.3.2 Cationic groups

The choice of cationic group is also of major importance in terms of creating a stable and long term working fuel cell. A variety of different cationic groups have been tested, e.g., simple quaternary ammonium ions (QA), cyclic QA, Guanidinium, Imidazolium, pyridinium, tertiary sulfonium, phosphonium, and metal cations such as ruthenium and cobaltcenium [13], see Figure 2.5 for structures of some of the mentioned cations. The QA will be the focus of further discussion of cation stability.

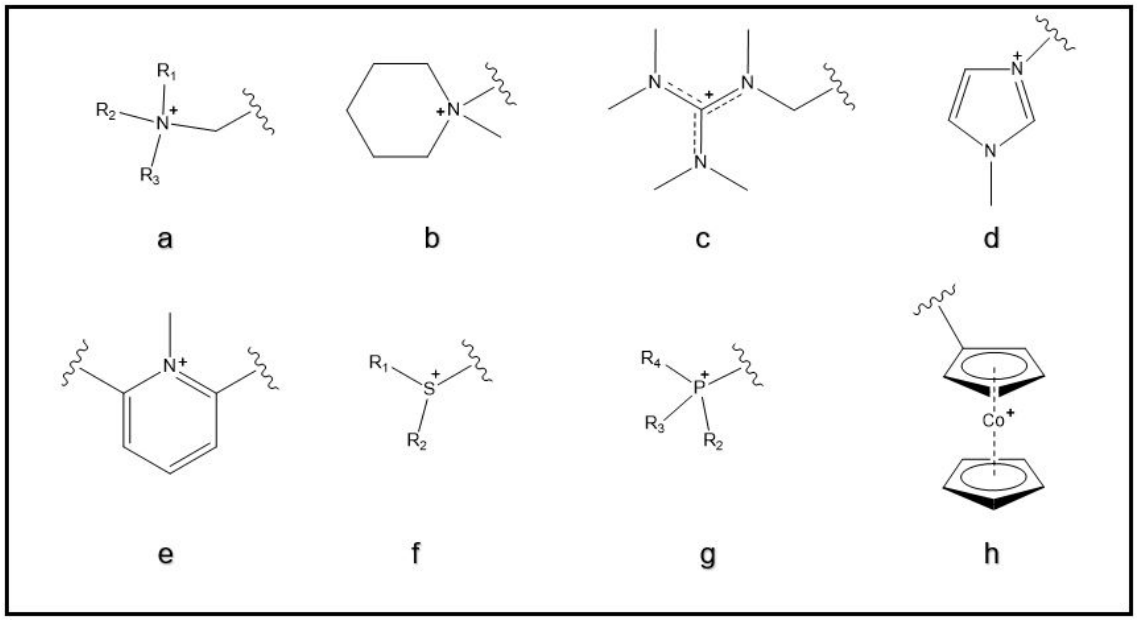

Figure 2.5 – Examples of cations used in AEMs. a: Simple QA, b: Cyclic QA, c: Guandinium, d: Imidazolium, e: Pyridinium, f: Solfonium, g: Phosphonium, h: Cobaltocenium. Adapted from ref. [1] and [21]

The cation can be connected to the backbone either by direct incorporation or tethering the cation to the backbone. The tethering can be done with or without an spacer. The benchmark QA cation is the tetramethylammonium (TMA), see Figure 2.8. How QA degrade in alkaline environment depends on the structure of the QA and how it is connected to the backbone.

The most common ways for QA to degrade is *via* Hofmann elimination and nucleophilic substitution but also ortho substitution, rearrangement reactions with benzyl ammonium compounds and Stevens rearrangement in the absence of β-hydrogens. The requirements for the Hofmann elimination are available β-hydrogens and an anti-periplanar conformation (180°) between the hydrogen and the leaving group. The reaction then goes through a transition state where 90° and 120° bond angles

are required (Figure 2.6) [10]. In nuclephilic substitution the hydroxide attacks the α-carbon and the the molecule goes via an trigonal bipyramidal transition state (figure 2.6). This requires access to the α-carbon and large substituents nearby can prevent the approach of OH^- [11].

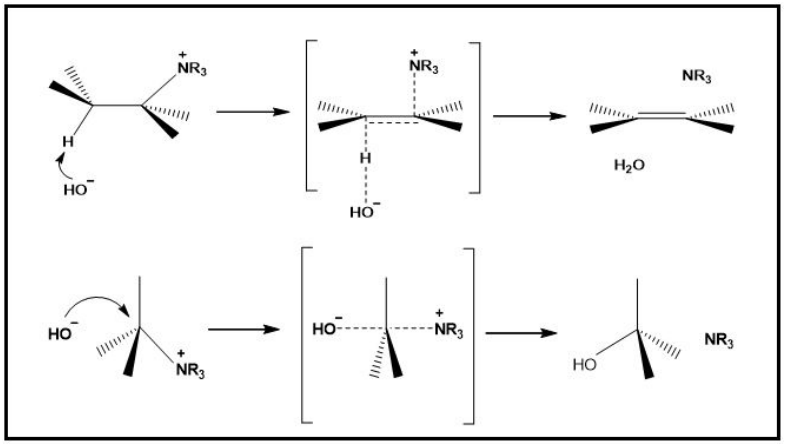

Figure 2.6 – Illustration of Hofmann elimination (top) and nucleophilic substitution (bottom)

These two are considered the major degradation pathways for QA but as mentioned earlier other degradation mechanisms can also be present and this depends on the structure of the QA and how it is attached to the polymer. These degradation reactions compete with each other and besides structure also depends on solvent and temperature. Elimination reactions are for example favoured by a higher temperature [11].

Effect of structure and linkage on alkaline stability for QA

For small molecule QAs, an aromatic structure seems to be less stable than a non aromatic one due to the planar structure, radical stabilization and acidity of nearby protons.

QAs attached *via* benzylic position is prone to degradation due to the electron-withdrawing effect and the electrophilicity of the QA. QAs attached via spacer chains instead of directly *via* benzylic position shows higher stability. This was a problem since one of the most common ways of functionalizing commercially available polymers resulted in QA attached *via* these type of bonds [10].

Side chain lengths of QA affects the stability. This was shown for QA of the structure $N(CH_3)_3R$, where R was an alkyl chain of varying length. The methyl group exhibits the highest stability due to the absence of β-hydrogens. The addition of a CH_2 group introduces β-hydrogens without any sterical hindrance and therefore decreases the stability. Additional CH_2 groups increases the stability up to the chain length of 6, thereafter it decreases. The decrease could be explained by more rapidly removed elimination products [10]. Not only does the chain length influence the stability of the cation, but also the structure of the attached chains or groups. In a study of small molecule QA, all attached to a benzyl group, ions with sterically hindered β-hydrogens and attached via spacers showed a higher stability than QAs that didn't have these protected β-hydrogens or spacers. In one study containing several different QA, three of these cations that had higher stability than the reference trimethylbenzylammonium (TMA). These cations were *N*-methyl-*N,N*-dipropylbenzylammonium (MnPr), *N*-methyl-*N,N*-dicyclohexylbenzylammonium (MCH) and
N,N,N-trimethyl-6-phenylhexylaminium (TMHA) (Figure 2.7). The stability was in order of TMHA>MCH>MnPr [12].

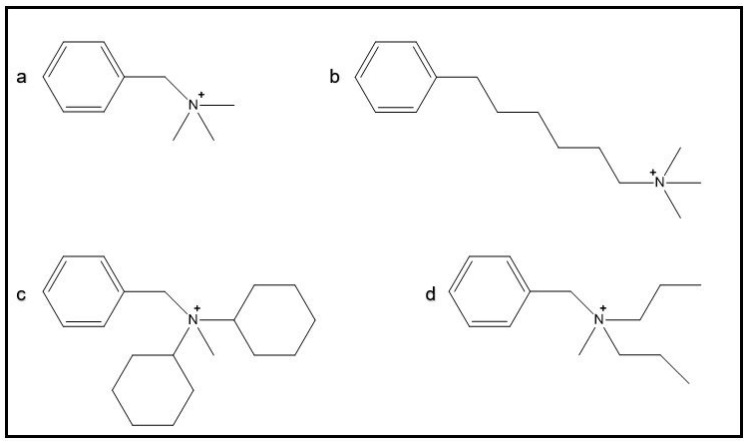

Figure 2.7 – QAs with different extender groups, a: TMA, b: TMHA, c: MCH, MnPr. Adapted from ref [12]

In another study examining the stability of small molecule QA, cyclic QAs such as dimethyl piperidine (DMP) and 6-azonia-spiro[5.5]undecane(ASU) showed higher stability than Tetramethylammonium (TMA). These three QA ions are shown in Figure 2.8. The high alkaline stability of the cyclic QA was ascribed to the unfavorable bond angles and lengths required in the transition states. The degradation of DMP occur mostly via methyl substitution but other possible degradation pathways such as ring-opening elimination and ring-opening substitution was also stated to be possible. Since ASU doesn't contain these methyl groups it also showed a higher stability and degraded *via* ring-opening substitution at the α-carbon [10].

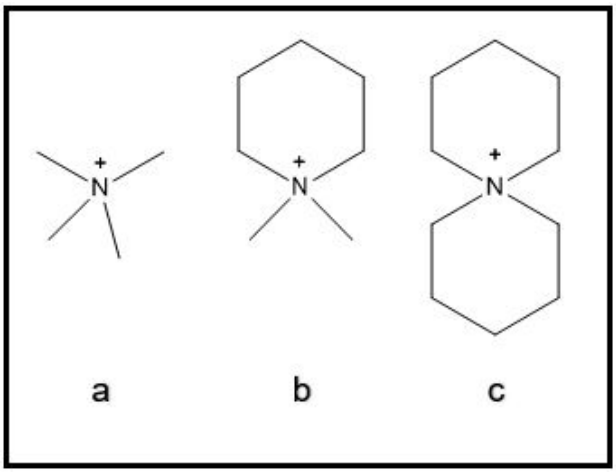

Figure 2.8 – Different QA ammonium. a: TMA (Tetramethylammonium), b: DMP, c: ASU

2.3.3 Synthesis of ether-free polymers incorporating cyclic QA

A way of preparing polymers without any labile aryl-ether bonds and incorporating cyclic QA has been developed based on reactions shown by Klumpp et al. They prepared diarylpiperidines through superelectrophilic activation. By using a superacid, in this case trifluoromethanesulfonic acid (TFSA) the reactivity of piperidone can be increased due to protonation of the ketone group and nitrogen. This dicationic species can then condense with aromatic compounds to yield the diarylpiperidines [8]. A polymer, poly(*p*-terphenyl *N*-methyl piperidinium) (Figure 2.9), without any labile aryl-ether bonds was synthesized by Joel et al. based on this type of reaction. In this superacid catalyzed polyhydroxyalkylation the propagation reaction competes with an elimination reaction that creates dead chain ends limiting the chain growth. Due to this propagation the reaction solution reached a maximum viscos-

ity which then decreased. This polymer were then further modified by converting the tertiary amine into a quaternary amine in Menshutkin reactions using varying length of alkylhalides, 1, 4, 6 and 8 carbons. The polymers degraded mostly via ring-opening Hofmann elimination and the polymers with longer extender chains showed poorer stability.. The polymer with the highest conductivity had a hexyl extender chain but this also had the second highest degradation rate. The polymers with shorter extender chains had a higher stability but a lower conductivity which was attributed to the large water uptake causing dilution effects [16]. This type of structure will be further investigated in this work with regards how the extender chains structure and size affects the water uptake, alkaline- and thermal stability and conductivity.

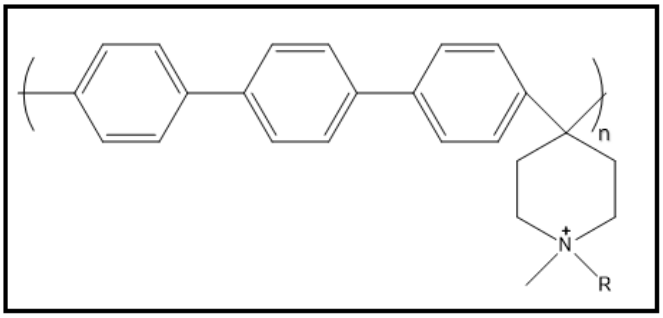

Figure 2.9 – The structure of Poly(*p*-terphenyl *N*-methyl-piperidinium) where R represents an alkyl chain with different lengths.

3 Experimental and methods

This work included polymerization of two different but structurally similar polymers which was then further functionalized by quaternization reactions involving different alkylhalides and a benzylic halide. Some of these materials were then further investigated as anion exchange membranes by measuring IEC, water uptake, conductivity and, thermal and alkaline stability.

3.1 Synthesis

3.1.1 Polymerization

The two superacid catalyzed polyhydroxyalkylation polymerization reactions carried out used a slightly modified procedure from [16]. The synthesis of poly(*p*-terphenyl piperidine) (PT-Pip) was carried out as following: *p*-terphenyl (2.9 g, 1 eq.), 4-piperidone monohydrate hydrochloride (2.1 g, 1.1 eq.) and DCM (11 ml, 14 eq.) were added to a three-neck round bottom flask with mechanical stirring. TFA (1.1 ml, 1.1 eq.) was then added to avoid excessive fuming. TFSA (11 ml, 9.8 eq.) was dropwise added. The reaction was carried out at 0 °C using a FT902 immersion cooler with ethanol as the coolant. The setup can be seen in Figure 3.1. The solution was left to react for 68 h until a high viscosity was observed. The solution was diluted with 70 ml of DMSO and then precipitated in water. The polymer was then filtered and washed in water, followed by toluene, followed by EtOH:diethylether 30:70.

Poly(*p*-terphenyl *N*-methylpiperidine) (PT-m-Pip) was prepared in a similar way described below:
p-Terphenyl (4 g, 1 eq.), *N*-methyl-4-piperidone (2.35 ml, 1.1 eq.) and DCM (15 ml, 14 eq.) were added to a three-neck round bottom flask followed by TFA (1.5 ml, 1.1 eq.) and dropwise addition of TFSA (15 ml, 9.7 eq.). The reaction was ended after 24 h. Direct precipitation could not be performed, instead the reaction solution was diluted with 90 ml DMSO and then precipitated in isopropanol:diethyl ether 50:50. The polymer was filtered and washed in aq. K_2CO_3, water and then toluene. The

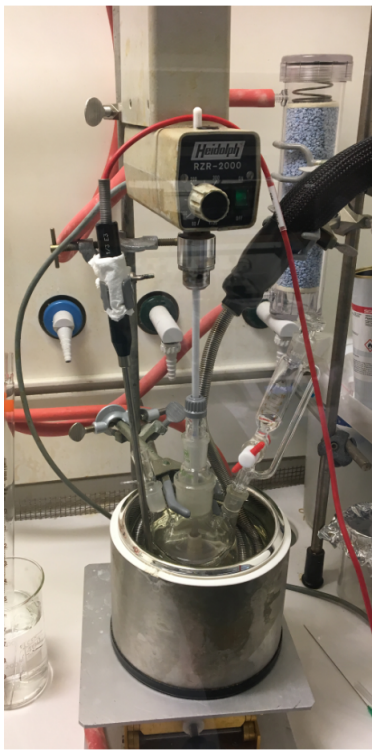

Figure 3.1 – Typical setup used in the polymerization reactions. The dropping funnel was, after addition of TFSA, replaced by a stopper

polymer was then dried at vacuum at 50 °C. The polymer was then washed in hot EtOH due to analysis showing monomer remaining in the polymer powder.

3.1.2 Quaternization

Quaternization of PT-Pip were attempted with the following alkylhalides and benzylic halide: 1-bromobutane, 1-bromohexane, 1-bromooctane, iodomethane, 1-bromo-2-methylpropane, (bromomethyl)cyclohexane and benzyl bromide.

A typical quaternization reaction of PT-Pip was carried out as follows: Polymer (0.5 g, 1 eq.) was dissolved in NMP (14 ml) alkylhalide (8 eq.) was then added followed by drop wise addition of a mixture consisting of NMP (3 ml) and DIPEA (0.7 ml, 2.5 eq.) which was done in order to prevent precipitation of the polymer caused by hydrogen bonding between secondary amine groups. Additional DIPEA (0.7 ml) was added 24 h later. The reactions were carried out at 80 °C and in a round bottom flask with magnetic stirring. The reactions were stopped and precipitated after evaluation of samples by ^{1}H NMR spectroscopy, which was done after 5-7 days.

In the case of iodomethane it was carried out in DMSO (6 ml) in the dark at RT using K_2CO_3 as the base. The reaction was stopped after 24 h. The polymers were precipitated in either water, ether, IPA or a mixture of the two latter. The quaternized polymers were then washed and dried at RT.

Quaternizations of PT-m-Pip were carried out as follows: polymer (0.6 g, 1 eq.), DMSO (6 ml), alkylhalide (3 eq.) and DIPEA (0.16 ml, 0.5 eq.) were added to a vial with magnetic stirring at 80 °C. K_2CO_3 (0.3 g, 0.5 eq.) were added 24 h after to ensure complete deprotonation of the polymer and thus complete quaternization. The reactions were stopped after evaluation of a sample using ^{1}H NMR spectroscopy, which was done after 4 days. The solutions were precipitated in different ratios of Isopropanol:diethyl ether. The precipitated polymers were washed, filtered and dried under vacuum at 50 °C for 48 h before the preparation of membranes.

Figure 3.2 shows the synthethic pathways of the polymerizations and subsequential quaternizations.

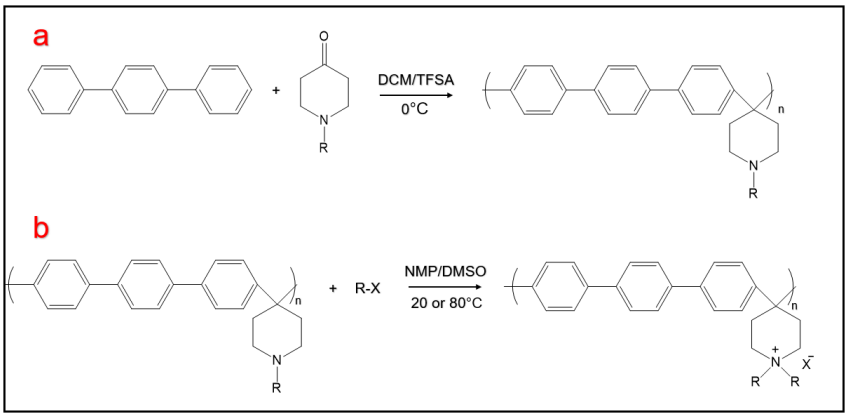

Figure 3.2 – Scheme of synthethic pathways. R represents either hydrogen or a carbon containing group. a shows the polymerization resulting in a polymer containing either a secondary or tertiary amine. b shows the quaternization reaction, R-X represents the alkylhalide or benzylic halide used. In the resulting polymer R is the same group or two different groups depending previous structure.

3.2 Membrane preparation

Membranes were prepared by dissolving 0.15 g of polymer (Br^- form) in 3 ml of DMSO and then filtering it through a teflon syringe filter (Millex 5 μm) onto a glass petri dish ($\varnothing$= 5 cm). The membranes were cast for 24-48 h at 80 °C. The cast membranes were hydrated with deionized water and then gently peeled of the dish and stored in deionized water until further analysis.

3.3 Characterization

3.3.1 Structural characterization using NMR)

The structure of the polymers was determined by proton nuclear magnetic resonance spetroscopy (^{1}H NMR spectroscopy) using a Bruker DR X400 spectrometer at 400.13 MHz with DMSO-d_6 as the solvent (δ = 2.50 ppm). 3-6 vol% TFA was added to shift the water peak (δ = 3.33 ppm before TFA) and to protonate any tertiary (or secondary) amines and therefore, enabling quantification and evaluation of quaternization and degradation. The protonation of amines results in a (often) distinguishable signal in the ^{1}H NMR spectra.

3.3.2 Viscosity measurements

The intrinsic viscosity ($[\eta]$) of PT-m-Pip in protonated form was determined using a Ubbeholde viscometer. The polymer was dissolved in DMSO with 0.1 M LiBr to avoid the polymer electrolyte effect. The flow time was measured for four different concentrations which were used to determine the reduced (η_{red}) and inherent (η_{inh}) viscosities using Eq. 3.1 and 3.2.

$$\eta_{red} = \frac{\frac{t_s}{t_b} - 1}{c} \tag{3.1}$$

$$\eta_{inh} = \frac{ln(\frac{t_s}{t_b})}{c} \tag{3.2}$$

t_b is the flow time of the blank sample and t_s is the flow time for polymer solution with a concentration of c. By extrapolating η_{red} and η_{inh} to c = 0 and taking the average value of the intersection with the y-axis the intrinsic viscosity is obtained.

3.3.3 Ion exchange capacity

The IEC of the quaternized polymers was determined by Mohr titration. The samples were dried under vacuum at 50 °C for 48 h. Approximately 0.03 g of each material, after drying, was put in 25 ml 0.2 M aq. $NaNO_3$ for 4 days at 60 °C. The solutions were then titrated using 0.01 M aq. $AgNO_3$ as titrant and 0.1N K_2CrO_4 as colorimetric indicator. Four titrations were done for each sample to avoid random errors.

3.3.4 Water uptake and swelling ratio

Water uptake of the AEMs was determined by taking the dry weight of a membrane in the Br^- form after drying under vacuum at 50 °C for 48 h. The membranes were then ion exchanged by immersing the membranes in ≈1 M aq. NaOH for 24-48 h under nitrogen atmosphere. The membranes were then washed in degassed deionized water and stored in degassed deionized water under nitrogen atmosphere overnight. The following day the membranes were equilibrated during the day at 20, 40, 60 and 80 °C. The membranes were then quickly wiped to remove excess water, weighted and measured. This procedure was used for each temperature. The absence of excess OH^- ions was controlled by a neutral pH of the water the membranes were stored in. To obtain good reference points for measuring swelling ratio the membranes were cut as illustrated in Figure 3.3

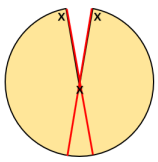

Figure 3.3 – Illustration how the membranes were cut in order to get reference points through- and in-plane swelling ratio. Thickness was obtained at the spots marked x and length along the red lines.

The dry weight of the membranes in OH^- form, W_{OH^-}, was calculated using the titrated IEC values and the dry weight of the membranes in Br^- form. The water

uptake of the swollen membranes, WU, were calculated using Eq. 3.3. $W^s_{OH^-}$ is the weight of the swollen membrane.

$$WU = \frac{W^s_{OH^-} - W_{OH^-}}{W_{OH^-}} \times 100\% \tag{3.3}$$

The hydration number (λ), the number of water molecules per OH^- in the membrane was calculated using Eq. 3.4

$$\lambda = \frac{(W^s_{OH^-} - W_{OH^-}) \times 1000}{M_{H_2O} \times IEC_{OH^-} \times W_{OH^-}} \tag{3.4}$$

3.3.5 Glass transition temperature T_g

Determination of T_g of PT-m-Pip was tried using differential scanning calorimetry (DSC) on a TA Instruments Q2000. The sample was dried under vacuum at 50 °for at least 24 h prior to analysis. The sample was heated from 20 to 360 °C, then cooled to 100 °C and subsequently heated again from 100 to 360 °C with a heating rate of 10 °C min$^-$1.

3.3.6 Thermal stability

The thermal stability of the polymers was studied by thermogravimetric analysis (TGA) using a TA Instruments TGA Q500. The samples were dried under vacuum at room temperature for 20 h prior to analysis. The samples were heated from 50 to 120 °C where they were held isothermally for 20 minutes to remove any remaining water. Subsequently the samples were heated from 50 to 600 °C with a heating rate of 10 °C min$^-$1. The temperature at 5% weight loss, $T_{d,95}$, was determined as the decomposition temperature. The measurements were done under a N_2 atmosphere.

3.3.7 OH^- Conductivity

The OH^- conductivity of the membranes were determined by electrochemical impedance spectroscopy at 20, 60, 40 and 80 °C by employing a Novocontrol high

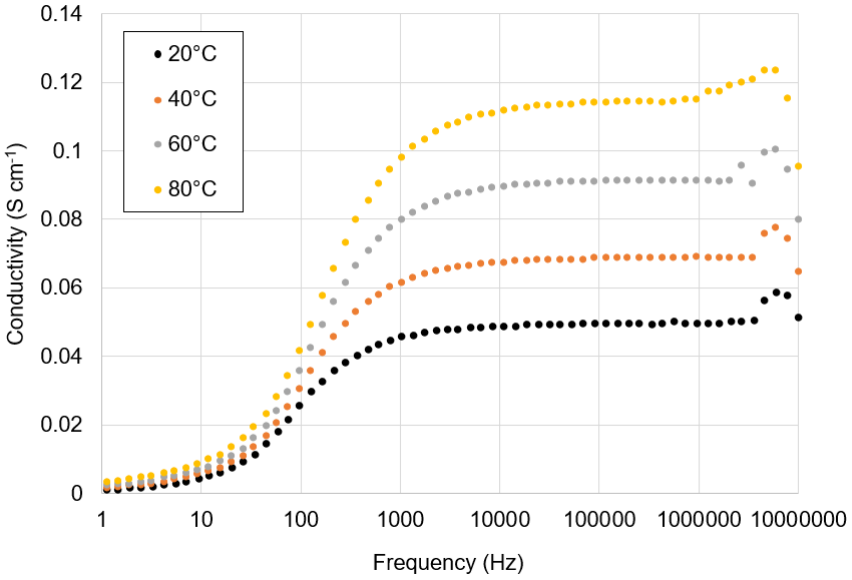

Figure 3.4 – Conductivity at 20, 40, 60 and 80 °C as a function of frequency. The conductivity values are obtained from the platue and corresponds to 50, 69, 91 and 114 mS cm^{-}1

resolution dielectric analyzer V 1.01S with voltage amplitude of 50 mV frequency varying between 10^0 to 10^7 Hz. The bulk resistance is measured at different frequencies and conductivity is then calculated by the instrument. For this calculation the thickness for the sample is needed. For each temperature a graph showing the conductivity as a function of frequency is obtained. The platue value in this graph is then taken as the ionic conductivity. See figure 3.4 for an example of this type of graph. During measurements the membranes were immersed in degassed deionized water in a sealed cell. Prior to analysis the membranes were ion exchanged from Br^- form to OH^- form and washed as described in previous water uptake and swelling ratio section. After washing and storing overnight in degassed water, under nitrogen, membranes were cut using the electrode from the analyzer as the template. The cut membranes were stored in degassed water under nitrogen prior to analysis. Due to further swelling, membranes were cut and thickness measured immediately prior to analysis.

3.3.8 Alkaline stability

To determine the alkaline stability the membranes were immersed in 2 M aq. NaOH in sealed containers at 90 °C. After predetermined times samples were taken out

and ion exchanged back to Br^- form by immersion of the samples in 1 M aq. NaBr. The samples were washed to remove excess Br^- ions and then dried under vacuum at 50 °C for 24 h. Degree of degradation of the sample was then determined by ^1H NMR spectroscopy described as earlier.

4 Results and Discussion

4.1 Polymerization

Two different polymers were prepared, Poly(*p*-terphenyl piperidine) denoted PT-Pip and Poly(*p*-terphenyl *N*-methylpiperidine) denoted PT-m-Pip. During the polymerization the solution turned blue/purple and the viscosity increased. The structure of the polymers was confirmed using ^{1}H NMR spectroscopy as described in the experimental section. The ^{1}H NMR spectra of PT-Pip and PT-m-Pip can be seen in Figure 4.1. The signal at 6.2 ppm originates from the inactive chain ends formed by the elimination reaction competing with the propagation reaction described in the background. This was expected but also unwanted. Both polymers when protonated were soluble in DMSO and NMP. PT-m-Pip in protonated form was also slightly soluble in hot MeOH and EtOH. Polymers in the nonprotonated form was insoluble in DMSO and NMP. The polymers in both forms were insoluble in water, diethylether and IPA. The protonated form of PT-Pip and the nonprotonated form of PT-m-Pip was insoluble in toluene.

For PT-Pip signals from the protons in the piperidine ring can be observed at 2.65 and 3.1 ppm. Signals from the aromatic protons can be observed at 7-8 ppm. Signals from protonated amines can be observed at 8.20-8.75 ppm. For PT-m-Pip signals from protons in the piperidine ring are observed between 2 and 3.8 ppm. signals from the aromatic protons are observed at 7-8 ppm. Signals from the protonated amine are observed at 9.5 ppm. At 6.2 ppm the signal from the protons due the elimination reaction can be observed.

Intrinsic viscosity was measured on PT-m-Pip in protonated form and resulted in a $[\eta] = 0.36$ dL g^{-1}. The polymer solution was not completely homogeneous due to impurities or particles so the solution was filtered before measurements which could have resulted in a loss of polymer and thus a lower intrinsic viscosity result.

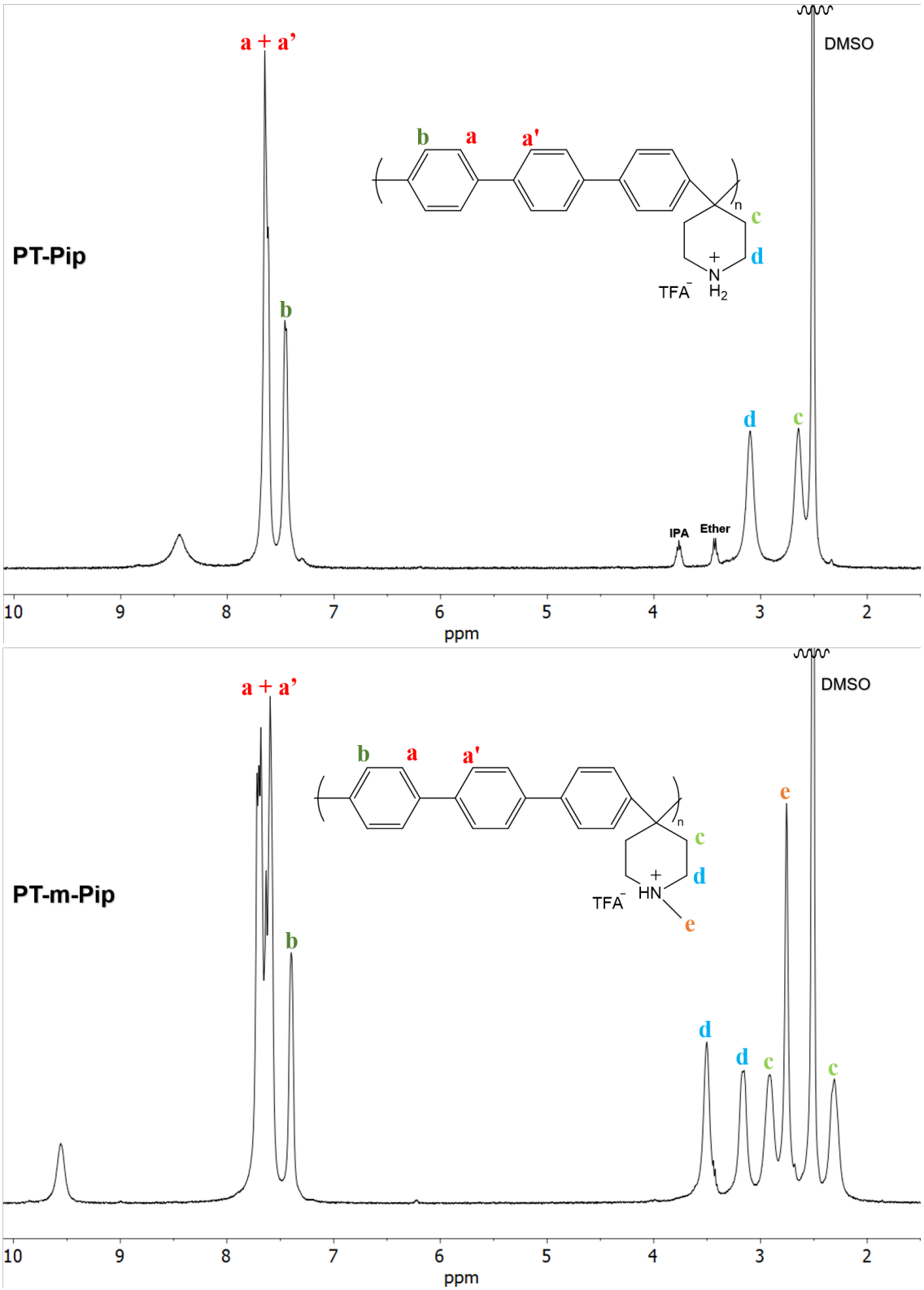

Figure 4.1 – ^{1}H NMR spectra of polymers PT-Pip (top) and PT-m-Pip (bottom) in DMSO-d_6 with 3-6 vol% TFA.

4.2 Quaternization

Quaternizations of the polymers (PT-Pip and PT-m-Pip) were evaluated using various alkylhalides and a benzylic halide. The tertiary amine polymer, PT-m-Pip, was succesfully quaternized using isobutylbromide (IBBr), (bromomethyl)cyclohexane (BrMCH) and benzyl bromide (BnBr) confirmed by ^{1}H NMR spectroscopy. The reaction solution were first heterogeneous and white but quickly turned homogeneous and the color changed from light yellow to orange as the reaction proceeded. These polymers are denoted PT-m-IB-Pip, PT-m-CHM-Pip and PT-m-Bn-Pip. The secondary amine polymer, PT-Pip, was succesfully quaternized using iodomethane, 1-bromobutane, 1-bromohexane, 1-bromooctane. This was confirmed by ^{1}H NMR spectroscopy (Figure 4.4). In the quaternization of PT-Pip, the reaction solutions changed color from light yellow to dark red as the reaction proceeded (Figure 4.2). Table 4.1 lists the polymers and which alkylhalide they were quaternized with and how the resulting polymers are denoted.

Polymer	Denoted	R-X	Quaternized polymer	Denoted
Poly(*p*-terphenyl N-methyl piperidine)	**PT-m-Pip**	Isobutylbromide	Poly(*p*-terphenyl-N,N-methyl-isobutyl piperidinium	**PT-m-IB-Pip**
		(Bromomethyl)cyclo hexane	Poly(*p*-terphenyl-N,N-methyl-cyclohexyl-methyl piperidinium)	**PT-m-CHM-Pip**
		Benzyl bromide	Poly(*p*-terphenyl-N,N-methyl-isobutyl piperidinium	**PT-m-Bn-Pip**
Poly(*p*-terphenyl piperidine)	**PT-Pip**	Iodomethane	Poly(*p*-terphenyl N,N-dimethyl piperidinium)	**PT-diMe-Pip**
		1-Bromobutane	Poly(*p*-terphenyl N,N-dibutyl piperidinium)	**PT-diBu-Pip**
		1-Bromohexane	Poly(*p*-terphenyl N,N-dihexyl piperidinium)	**PT-diHe-Pip**
		1-Bromooctane	Poly(*p*-terphenyl N,N-dioctyl piperidinium)	**PT-diOc-Pip**

Table 4.1 – Table listing the two polymers, how they are denoted, which alkylhalide they were quaternized with (R-X) and the resulting polymer and how it is denoted in this work. For structures, see Figure 4.4, 4.10, 4.11 and 4.12

Successful quaternization was verified by the absence of signals corresponding to protonated amines and a correct ratio between the intensities of the signals originating from to aromatic protons, the piperidine ring and the extender groups. PT-Pip was harder to work with due to the occasional precipitation of the polymer in the reaction solutions. The solution then became a gel which hindered stirring and mixing. This precipitation was most likely due to hydrogen bonding between secondary amine groups which resulted in a decreased solubility of the polymer.

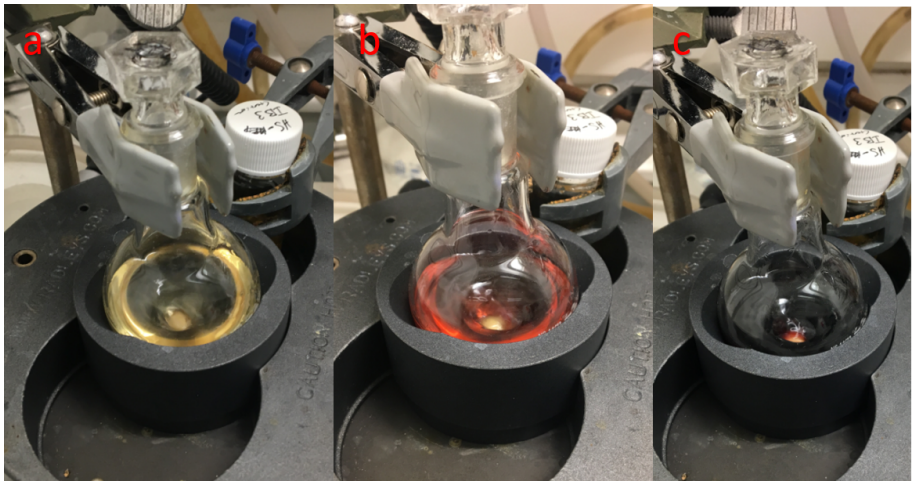

Figure 4.2 – Color change of a quaternization reaction of PT-Pip with 1-Bromooctane. a) at the start of the reaction, b) after 30 minutes, c) after 12 h.

Quaternization of PT-Pip using isobutylbromide, (bromomethyl)cyclohexane and benzyl bromide resulted in polymers containing tertiary amine groups i.e. the quaternization was unsuccessful. The unsuccessful quaternization of PT-Pip using IBBr, BrMCH and BnBr is most likely due to steric hindrance. This was shown by ^{1}H NMR spectroscopy (Figure 4.3) of a reaction that had been going on for 17 days between PT-Pip and IBBr. Signals from the protonated amine can still be observed and the ratio between aromatic and the protons in the extender chain indicate that there is only one extender chain on the piperidine.

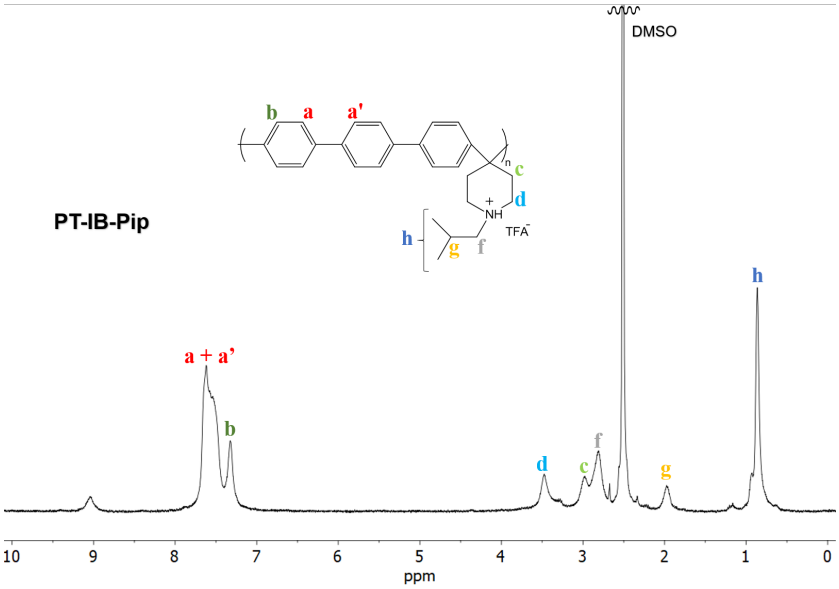

Figure 4.3 – ^{1}H NMR spectrum of the product from quaternization attempt of PT-Pip with isobutylbromide in DMSO-d_6 with 3-6 vol% TFA

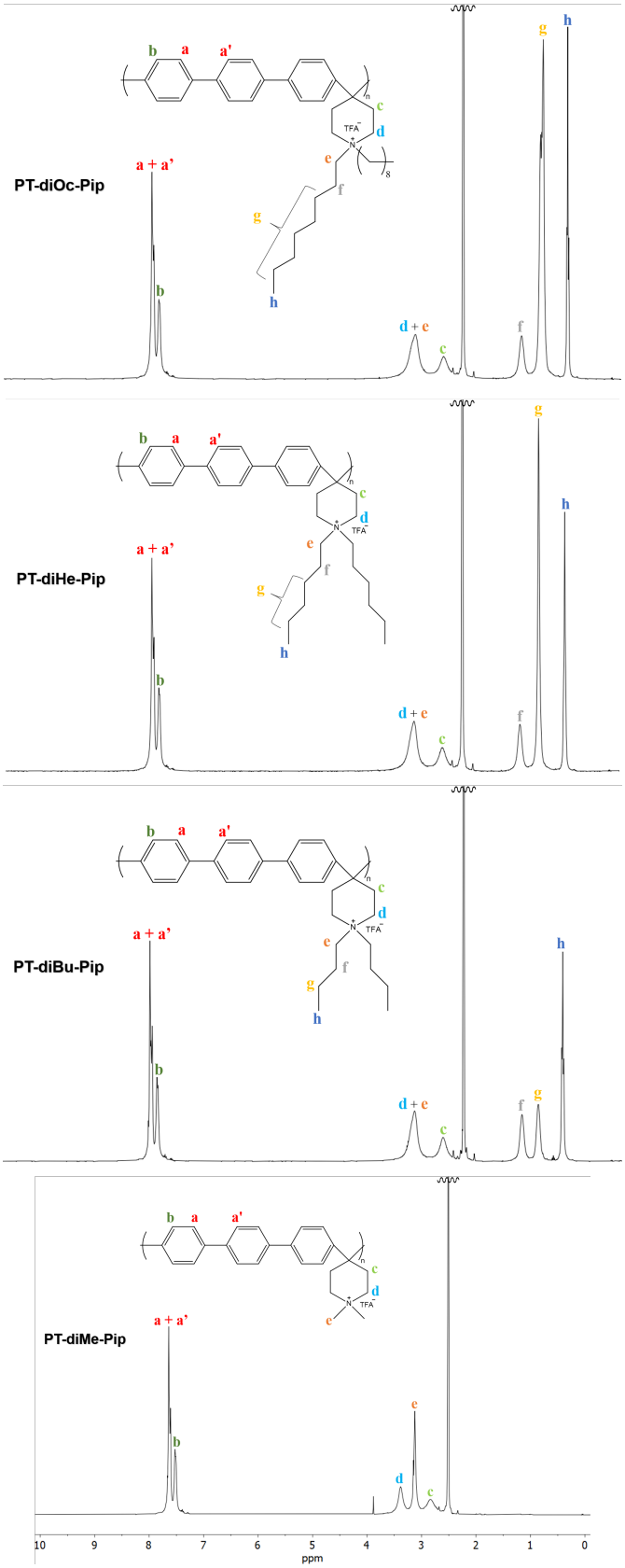

Figure 4.4 – ^{1}H NMR spectrum NMR spectra of PT-DiOc-Pip, PT-DiHe-Pip, PT-DiBu-Pip, PT-DiMe-Pip in DMSO-d_6 with 3-6 vol% TFA

4.3 Membrane casting

Membranes of successfully quaternized polymers were cast from solutions containing 5 wt% polymer in DMSO at 80°C. All polymers formed flexible and transparent membranes of varying degree except for PT-diBu-Pip, PT-DiOc-Pip which were brittle and cracked. Additional images of cast membranes can be seen in appendix 1. After casting membranes of the PT-diXX-Pip polymers, NMR spectra showed that they still contained *p*-terphenyl residue. The membranes and remaining polymer were then washed in hot MeOH and hot EtOH but were slightly soluble and therefore a significant amount of the material was lost. Further characterizations of these materials were, therefore, not continued due to time constraints. Figure 4.5 shows an example of a successfully cast membrane which was also further characterized.

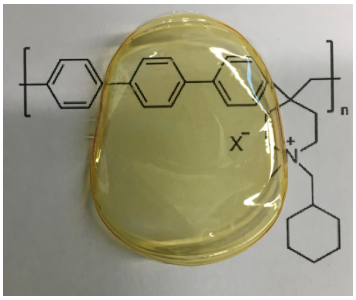

Figure 4.5 – AEM of the polymer PT-m-CHM-Pip

4.4 Membrane characterization

The polymers that were further investigated as anion exchange membranes were PT-m-IB-Pip, PT-m-CHM-Pip and PT-m-Bn-Pip. Complete quaternization of these further investigated materials was, in addition to ^{1}H NMR spectroscopy, also confirmed by Mohr titration. Properties of the AEMs are shown in Table 4.2 at the end of this section.

4.4.1 Thermal stability

The thermal stability of AEMs and the precursor polymer (PT-m-Pip) were evaluated using TGA. $T_{d,95}$ was 252, 250, 272 and 422 °C for PT-m-IB-Pip, PT-m-CHM-Pip, PT-m-Bn-Pip and PT-m-Pip respectively (Figure 4.6). The $T_{d,95}$ is the lowest for PT-m-CMH-Pip due to the higher aliphatic content. PT-m-IB-Pip shows

a slightly lower one due to lower aliphatic content compared to PT-m-CHM-Pip. PT-m-Be-Pip shows a higher $T_{d,95}$ which is attributed to the more thermally stable benzyl group.

DSC was also run on the precursor polymer PT-m-Pip. No glass transition temperature could be detected within the examined temperature interval. T_g of a polymer of the same structure has been reported to be 320 °C [16].

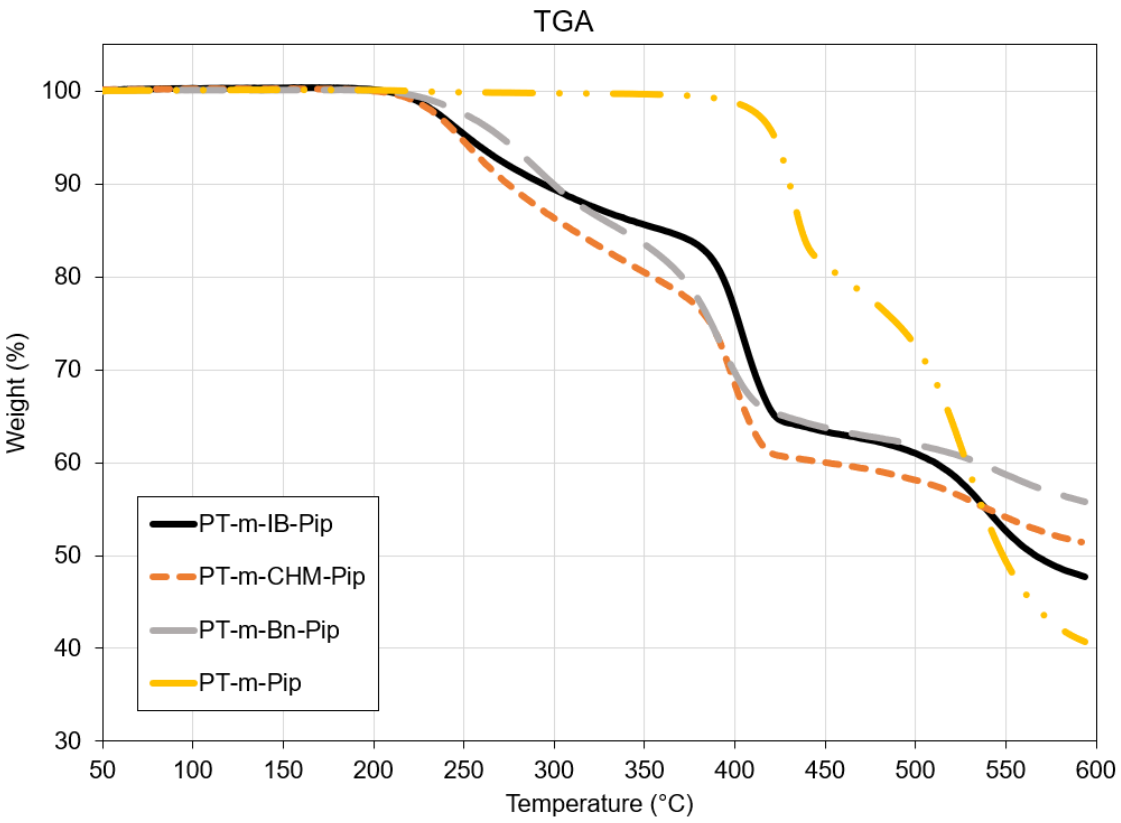

Figure 4.6 – TGA traces of AEMs and PT-m-Pip measured at 10 °C min⁻1 under nitrogen atmosphere

4.4.2 Water uptake

The water uptake was evaluated at 20, 40, 60 and 80 °C (Figure 4.7). The water uptake increased with both temperature and IEC as expected. At 80 °C the water uptake reached 202, 264 and 316 wt% for PT-m-CHM-Pip, PT-m-Bn-Pip and PT-m-IB-Pip respectively. The water uptake for all polymers were higher than similar polymers from ref [16] with the same IEC. This difference could be due to polymers in this work having a lower molecular weight or a different cation structure.

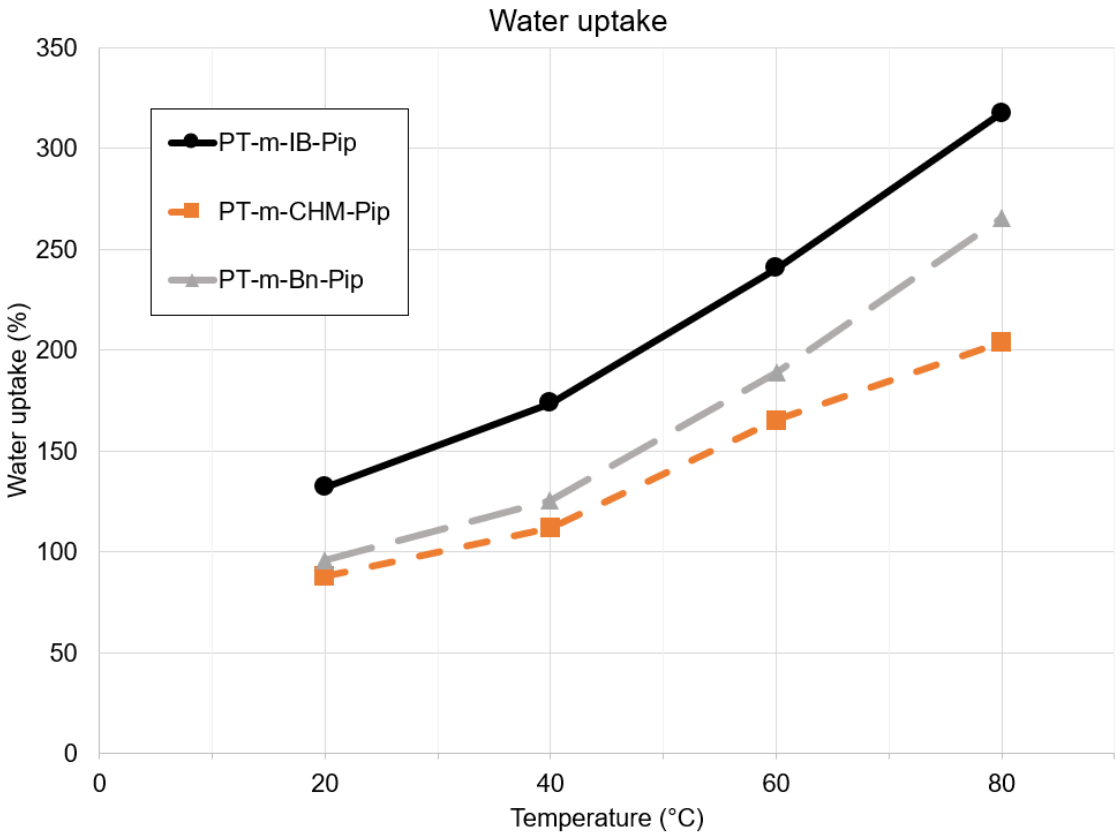

Figure 4.7 – Water uptake by the AEMs in OH^- form

In order to obtain reference points to measure the swelling ratio (SR), the membranes were cut as described in 3.3. This unfortunately led to two of the membranes (PT-m-IB-Pip and PT-m-Bn-Pip) being damaged during the 80 °C measurement (they were torn apart). However, this did not influence the measurements.

4.4.3 Conductivity

The OH^- conductivity for the different materials was evaluated for 20, 40, 60 and 80 °C (figure 4.8). The highest conductivity at 80 °C was reached by PT-m-CHM-Pip at 107 mS cm^-1, followed by PT-m-IB-Pip at 105 mS cm^-1 and PT-m-Be-Pip at 103 mS cm^-1. This did not follow the IEC but too few measurements were probably done (3 for each structure) and an extended amount of time exposed to air due the need for cutting the membranes into the right dimensions prior to the measurements probably affected the results. The highest conductivity for a single sample of each polymer was 122, 114 and 107 mS cm^-1 for PT-m-IB-Pip, PT-m-CHM-Pip and

PT-m-Bn-Pip respectively.

The conductivity for PT-m-IB-Pip can be compared to the structure of PT-m-butyl-Pip which have a reported conductivity of 84 mS cm^{-}1[16]. This could be attributed to a higher water uptake or that the structure of the extender group somehow affects the association and dissociation of the hydroxide ion.

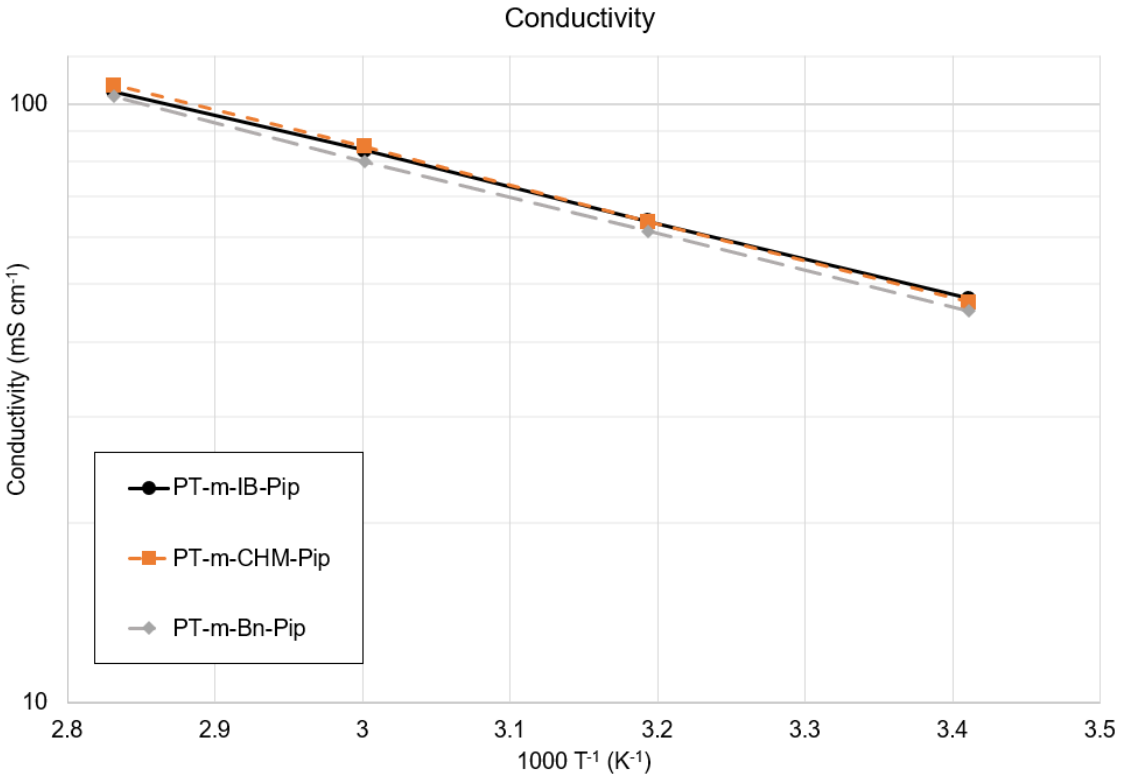

Figure 4.8 – Conductivity plot of the membranes in OH^{-} form

4.4.4 Alkaline stability

The possible degradation pathways for the polymers can be seen in Figure 4.9. In PT-m-Bn-Pip the abscence of β-hydrogens in the extender groups made pathway b) impossible.

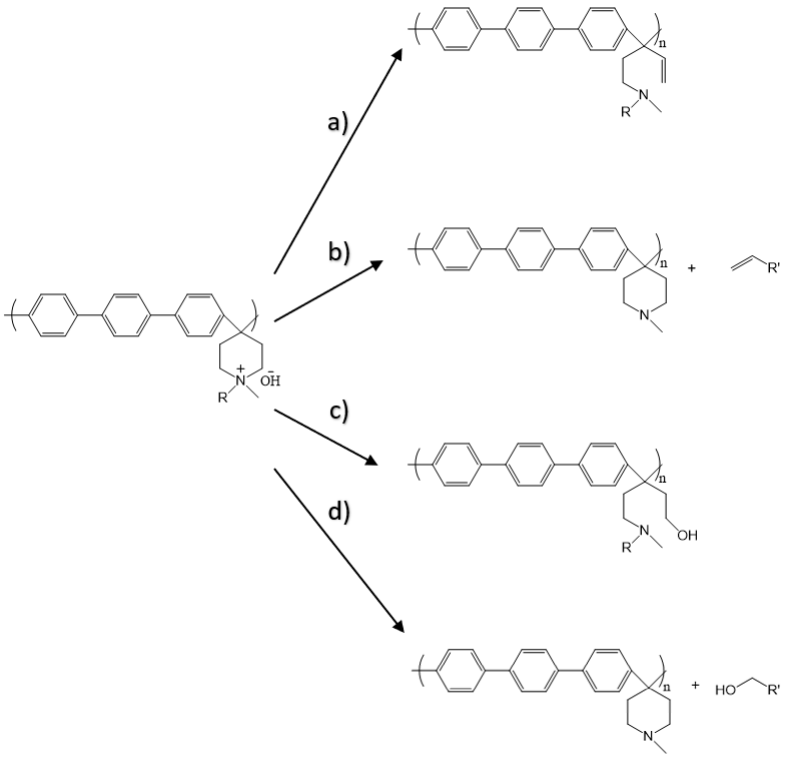

Figure 4.9 – Possible degradation pathways for the polymers. a: Hofmann ring-opening elimination, b: Hofmann elimnation in the extender group, c: Ring-opening nucleophilic substutition, d: Nuclephilic substitution in the extender chain.

In Figures 4.10, 4.11 and 4.12, the ^{1}H NMR spectra can be seen for the three polymers prior and after immersion in 2 M NaOH aq. for 360 h at 90 °C.

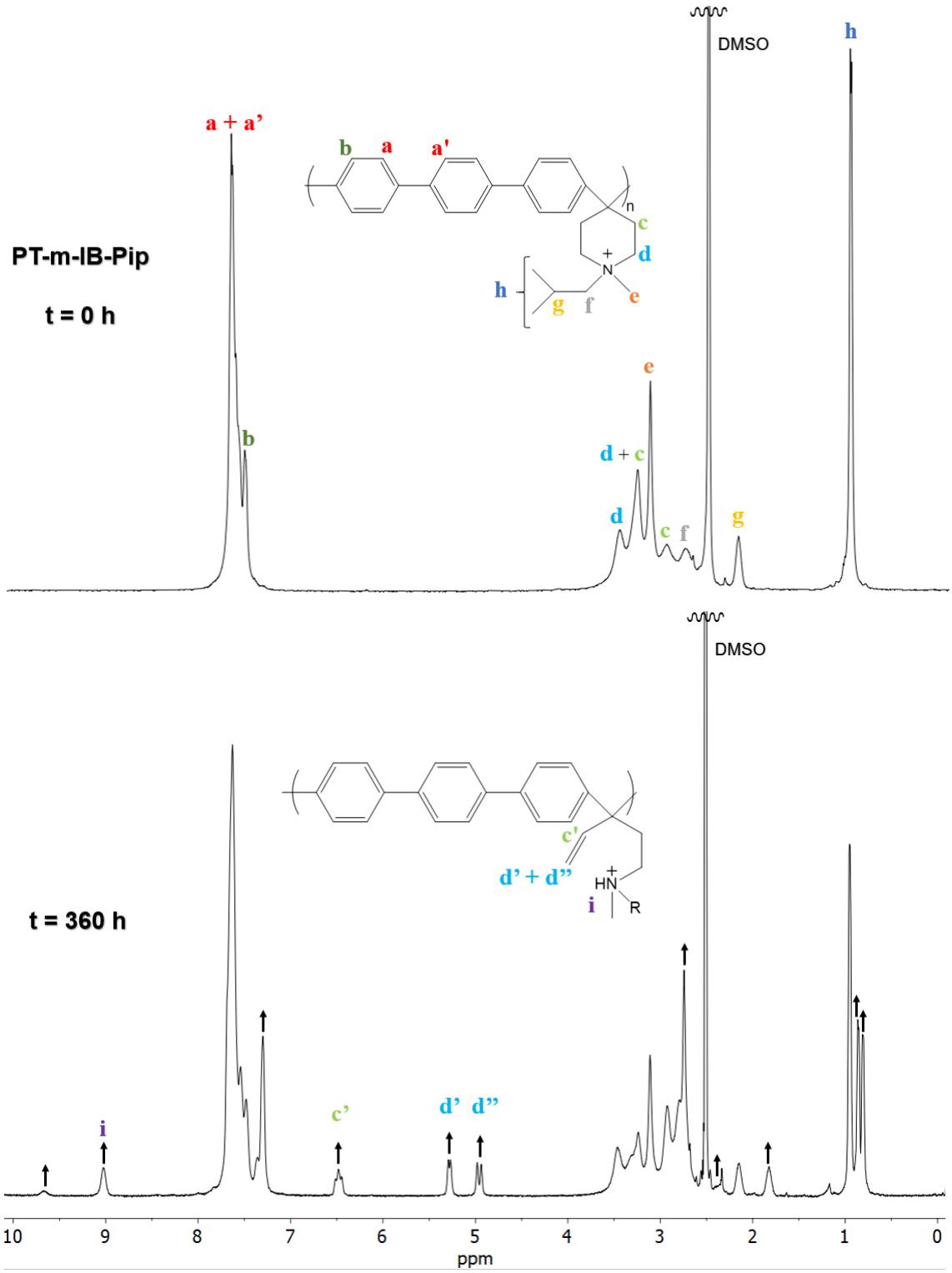

Figure 4.10 – ^{1}H NMR spectra of PT-m-IB-Pip in DMSO-d_6 with 3-6 vol% TFA before and after immersion during 360 h in 2 M NaOH aq. at 90 °C.

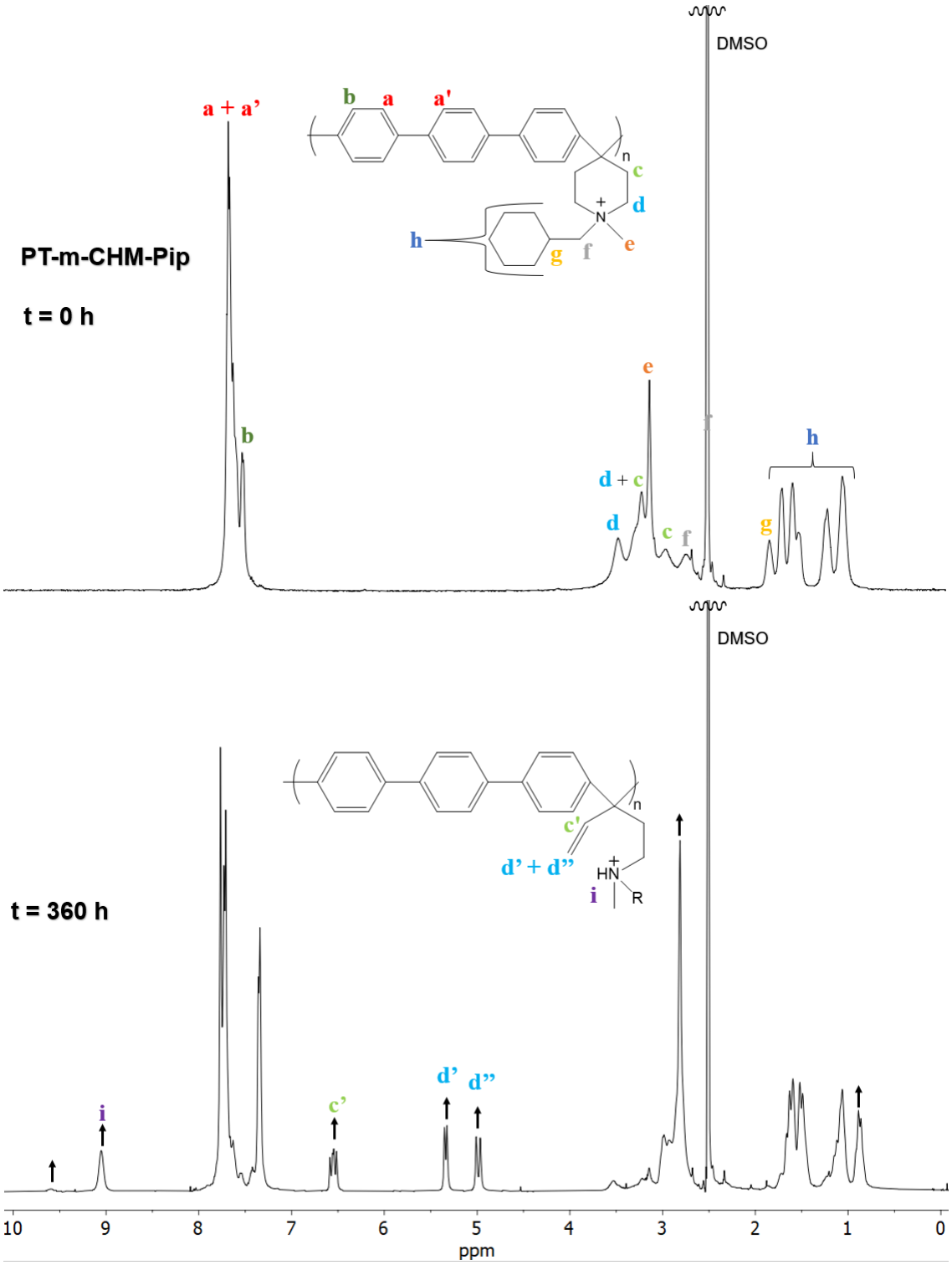

Figure 4.11 – ^{1}H NMR spectra of PT-m-CMH-Pip in DMSO-d_6 with 3-6 vol% TFA before and after immersion during 360 h in 2 M NaOH aq. at 90 °C.

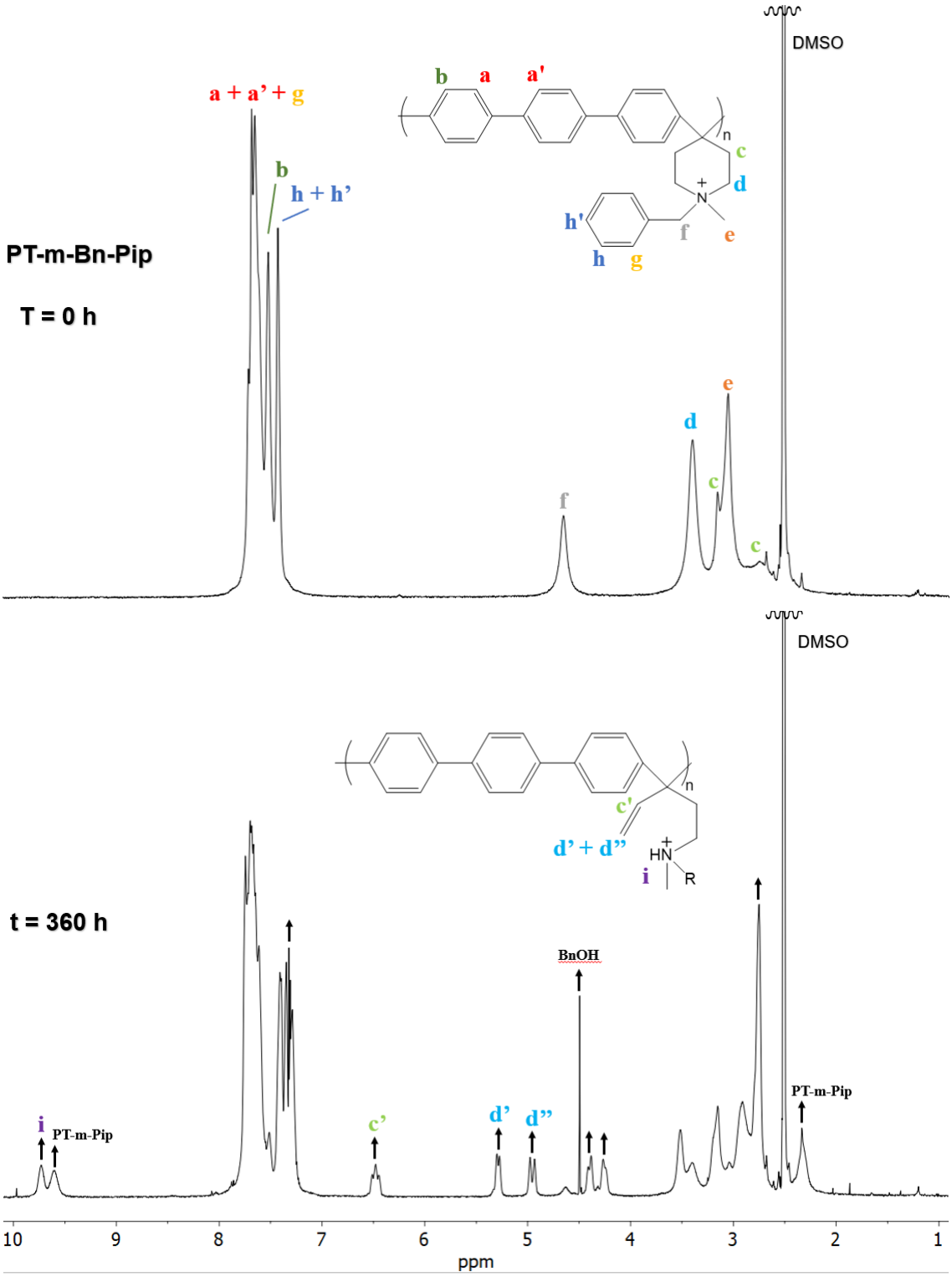

Figure 4.12 – ^{1}H NMR spectra of PT-m-CMH-Pip in DMSO-d_6 with 3-6 vol% TFA before and after immersion during 360 h in 2 M NaOH aq. at 90 °C.

Degradation could be observed by the reappearance of signals originating from protonated amines observed at 9 ppm and above, depending on polymer. Degradation through Hofmann in the ring can be observed for all polymers by the appearance of signals at around 5, 5.3 and 6.6 ppm believed to originate from vinylic protons. This was as expected to be the main degradation pathway for PT-m-IB-Pip and PT-m-CHM-Pip.

For PT-m-IB-Pip (Figure 4.10) a reduced intensity of signals at 0.7 - 1 ppm originating from the primary carbons on the isobutyl chain and indicates a loss of the isobutyl extender chain, either through nucleophilic substution or Hofmann elimination. The loss in intensity almost corresponded to the signal at 9.7 ppm. Also the reappearance of a signal at 2.4 ppm which could belong to the structure of the precursor polymer PT-Pip also indicates this. In the spectra of PT-m-CHM-Pip (Figure 4.11) a similar peak at 9.6 ppm originating from a protonated amine can be observed indicating at least one additional degradation pathway for this polymer. For PT-m-Bn-Pip (Figure 4.12) degradation through nucleophilic substition at the benzylic carbon is indicated by the reappearance of protons originating from the piperidine ring at 2.3 ppm but also from signals likely originating from benzyl alcohol at 4.5 ppm. Two different slightly overlapping signals from protonated amines could be observed at 9.6 and 9.7 which indicates two degradation pathways for this polymer.

The total degradation for PT-m-IB-Pip and PT-m-CHM-Pip (Figure 4.13) was evaluated by integration and comparison of the intensity of the signals originating from the protonated amines, with the signals of aromatic protons. The amount of degradation through Hofmann in the ring was obtained in a similar way by comparing the signals at 5, 5.3 and 6.6 ppm to the signals of the aromatic protons. For PT-m-Bn-Pip this was not possible due to the loss of benzyl extender groups *via* nucleophilic substitution at the benzylic carbon. Since this results in a decrease of the signals of the aromatic protons these cannot be used as a reference like for the other two polymers. Since the two most likely degradation pathways for this polymer are both Hofmann in the ring and nucleophilic substution at the benzylic carbon at least these two could be compared to see which one dominates under these conditions. Comparison between the signals arising from Hofmann and the total degradation showed that these degradation through these pathways seemed to be of equal magnitude.

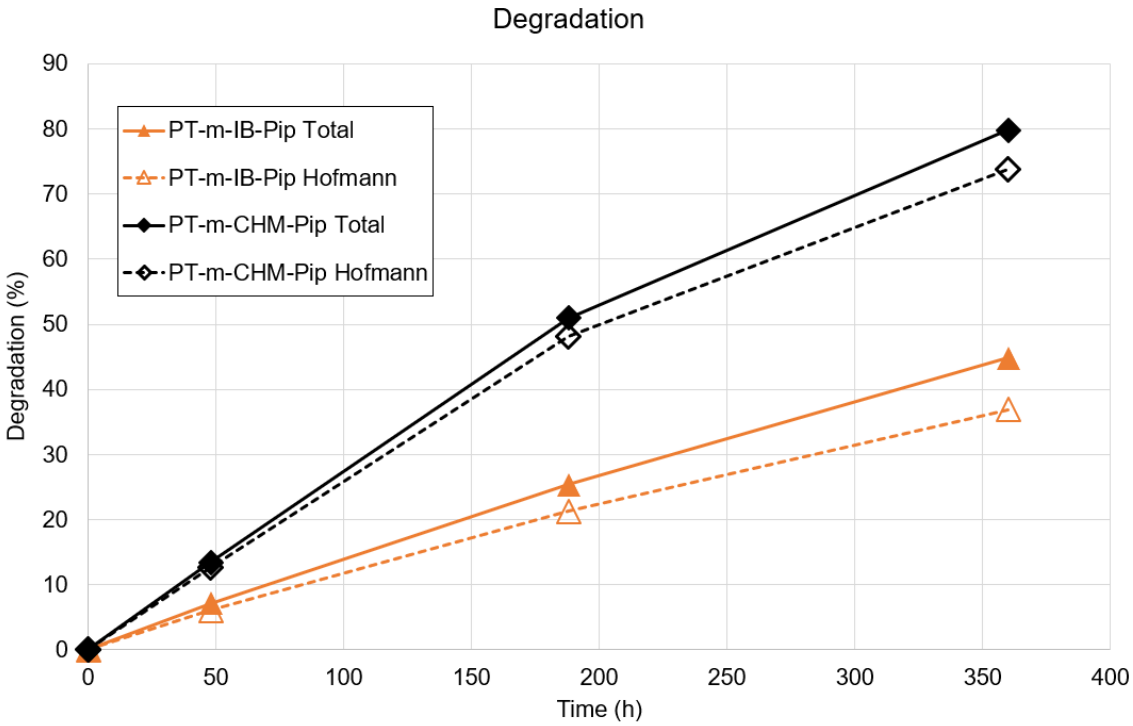

Figure 4.13 – Cationic loss as a function of time for PT-m-IB-Pip and PT-m-CHM-Pip. Closed symbols and solid lines represent total degradation. Open symbols and dashed lines represent degradation through Hofmann ring-opening elimination.

The high degree of Hofmann in the ring was also observed in previous mentioned studies [16] and was ascribed to the unfavorable confirmations the piperidine ring is locked into in this type of structure which may restrict ring relaxation. This is supported by the fact the PT-m-IB-Pip showed a higher degradation rate than the counterpart with a linear extender chain (25% degradation 360 h) and the degradation rate of PT-m-CHM-Pip was also higher than comparable structures in the same study (around 60% after 360 h).

Table 4.2 – Properties of the AEMs. a) Calculated from the polymer structure in Br^- form, OH^- form within paranthesis; b) Water uptake at 80 °C in OH^- form; c) Swelling ratio calculated at 20 °C in OH^- form; d) OH^- conductivity of fully hydrated (immersed) AEM at 80 °C

	IEC_{Br} (meq. g^{-1})							
Polymer	Theoretical[a]	Titrated	$WU_{OH,80\ °C}$[b] *(wt%)*	$\lambda_{OH,80\ °C}$[b]	$SR_{OH,\ 20\ °C}$[c] in-plane (%)	$SR_{OH,\ 20\ °C}$[c] through-plane (%)	$\sigma_{OH,80\ °C}$[d] *(mS cm^{-1})*	$T_{d,95}$ (°C)
PT-m-IB-Pip	2.16 (2.50)	2.21	318	70	38	27	105	252
PT-m-CHM-Pip	1.99 (2.28)	2.10	204	50	20	18	107	250
PT-m-Bn-Pip	2.01 (2.31)	2.08	266	64	19	17	103	272

5 Conclusion

Poly(*p*-terphenyl piperidinium) was synthesized and functionalized with seven different extender chains. Three additional extender chains were evaluated but were unsuccessful due to the sterical restriction and size of the extender chains. AEMs were prepared from three of these successfully synthesized polymers and further analysed by measuring water uptake, thermal and alkaline stability and conductivity.

Of the three AEMs, the one with the largest extender group, PT-m-CHM-Pip showed the highest conductivity and the lowest water uptake. However, it also had low alkaline stability and the lowest thermal stability. The AEM with the smallest extender group showed the second highest conductivity and the highest alkaline stability, however, it had a large water uptake. The AEM with the benzyl extender group showed the highest thermal stability but the lowest conductivity and low alkaline stability.

All of the three AEMs showed relatively high conductivity. Comparison between these three AEMs, and AEMs from other studies based on the poly(*p*-terphenyl *N*-methylpiperidinium) structure with comparable IEC, suggests that there is an effect of the extender groups structure on the conductivity and water uptake. The higher water uptake and conductivity of the AEMs in this work could result from a higher dissociation of the hydroxide ion or a different morphology, both as a result of the structure of the extender group.

This work also showed that a large extender group attached to the piperidinium ring can cause a decrease in the alkaline stability. This further confirms the importance of careful incorporation of these cations into polymers, in order to enable ring strain relaxation.

Finally, the work also gives an insight regarding the stability of the benzylic position in comparison with the stability of the piperidinium ring in the poly(*p*-terphenyl N-

methylpiperidinium) structure.

6 Future Work

The original aim was to synthesize and evaluate the disubstituted structures. However, this was not possible due to solubility issues, etc. It would be interesting to evaluate the disubstituted structures in a future work. To simplify the synthesis and mitigate the problem with solubility working with copolymers would be recommended.

Additional extender groups that could be interesting to investigate in the PT-m-pip structure would be 2-bromopropane, 1-bromo-3-ethylpentane, 2-ethylbutyl bromide or 3-(bromomethyl)-2,4-dimethylpentane. This would be interesting since these polymers would result in different structures of the piperidinium cation, but with IEC comparable to the structures evaluated in this work and previous studies.

Characterization of the AEMs should also be done with SAXS to evaluate the morphology and phase separation.

Tethering piperidinum cations, with similar structures as the ones evaluated in this work, further away from the backbone would also be useful to further understand the importance of enabling ring strain relaxation in the type of cyclic QA used in this work and previous studies.

References

[1] Christopher G. Arges and Le Zhang. "Anion Exchange Membranes' Evolution toward High Hydroxide Ion Conductivity and Alkaline Resiliency". In: *ACS Applied Energy Materials* 1.7 (2018), pp. 2991–3012. DOI: 10.1021/acsaem.8b00387. eprint: https://doi.org/10.1021/acsaem.8b00387.

[2] Pia Aßmann et al. "Toward developing accelerated stress tests for proton exchange membrane electrolyzers." In: *Current Opinion in Electrochemistry* 21 (2020), pp. 225–233. ISSN: 2451-9103.

[3] Dario R. Dekel. "Review of cell performance in anion exchange membrane fuel cells". In: *Journal of Power Sources* 375 (2018), pp. 158–169. ISSN: 0378-7753. DOI: https://doi.org/10.1016/j.jpowsour.2017.07.117.

[4] C.E. Diesendruck and D.R. Dekel. "Water - A key parameter in the stability of anion exchange membrane fuel cells." In: *Current Opinion in Electrochemistry* 9 (2018), pp. 173–178.

[5] Shimshon Gottesfeld et al. "Anion exchange membrane fuel cells: Current status and remaining challenges." In: *Journal of Power Sources* 375 (2018), pp. 170–184. ISSN: 0378-7753.

[6] K.F.L. Hagesteijn, Jiang Shanxue, and B.P. Ladewig. "A review of the synthesis and characterization of anion exchange membranes." In: *Journal of Materials Science* 53.16 (2018), pp. 11131–11150.

[7] Mohammad Bagher Karimi, Fereidoon Mohammadi, and Khadijeh Hooshyari. "Recent approaches to improve Nafion performance for fuel cell applications: A review." In: *International Journal of Hydrogen Energy* 44.54 (2019), pp. 28919–28938. ISSN: 0360-3199.

[8] Douglas A. Klumpp et al. "Synthesis of Aryl-Substituted Piperidines by Superacid Activation of Piperidones". In: *The Journal of Organic Chemistry* 64.18 (1999). PMID: 11674674, pp. 6702–6705. DOI: 10.1021/jo990454i. eprint: https://doi.org/10.1021/jo990454i.

[9] James Larminie. "Fuel Cells". In: *Kirk-Othmer Encyclopedia of Chemical Technology*. American Cancer Society, 2002. ISBN: 9780471238966. DOI: 10.1002/0471238961.0621051211091415.a01.pub2. eprint: https://onlinelibrary.wiley.com/doi/pdf/10.1002/0471238961.0621051211091415.a01.pub2.

[10] M. G. Marino and K. D. Kreuer. "Alkaline Stability of Quaternary Ammonium Cations for Alkaline Fuel Cell Membranes and Ionic Liquids". In: *ChemSusChem* 8.3 (2015), pp. 513–523. DOI: 10.1002/cssc.201403022. eprint: https://onlinelibrary.wiley.com/doi/pdf/10.1002/cssc.201403022.

[11] Michael G. Marino. *Anion exchange membranes for fuel cells andgflow batteries: Transport and stability of model systems.* Max-Planck-Institut fur Festkorperforschung, 2015. ISBN: 9789174227390.

[12] Angela D. Mohanty and Chulsung Bae. "Mechanistic analysis of ammonium cation stability for alkaline exchange membrane fuel cells". In: *J. Mater. Chem. A* 2 (41 2014), pp. 17314–17320. DOI: 10.1039/C4TA03300K.

[13] Angela D. Mohanty et al. "Systematic Alkaline Stability Study of Polymer Backbones for Anion Exchange Membrane Applications". In: *Macromolecules* 49.9 (2016), pp. 3361–3372. DOI: 10.1021/acs.macromol.5b02550. eprint: https://doi.org/10.1021/acs.macromol.5b02550.

[14] Ziv Noga and Dekel Dario R. "A practical method for measuring the true hydroxide conductivity of anion exchange membranes." In: *Electrochemistry Communications* 109-113 (2018), p. 109. ISSN: 1388-2481.

[15] Joel S. Olsson. *Exploring N-alicyclic quaternary ammonium functional polymers as hydroxide exchange membranes.* Centre for Analysis and Synthesis, Department of Chemistry, Lund University, 2020. ISBN: 9789174227390.

[16] Joel S. Olsson, Thanh Huong Pham, and Patric Jannasch. "Poly(arylene piperidinium) Hydroxide Ion Exchange Membranes: Synthesis, Alkaline Stability, and Conductivity". In: *Advanced Functional Materials* 28.2 (2018), p. 1702758. DOI: 10.1002/adfm.201702758. eprint: https://onlinelibrary.wiley.com/doi/pdf/10.1002/adfm.201702758.

[17] Shruti Prakash, William E. Mustain, and Paul A. Kohl. "Chapter 1 - Electrolytes for Long-Life, Ultra Low-Power Direct Methanol Fuel Cells." In: *Micro Fuel Cells* (2009), pp. 1–50. ISSN: 978-0-12-374713-6.

[18] Yan-Jie Wang et al. "Alkaline polymer electrolyte membranes for fuel cell applications." In: *CHEMICAL SOCIETY REVIEWS* 42.13 (2013), pp. 5768–5787. ISSN: 03060012.

[19] J.-H. Wee. "Applications of proton exchange membrane fuel cell systems." In: *Renewable and Sustainable Energy Reviews* 11.8 (2007), pp. 1720–1738. ISSN: 13640321.

[20] Michael M. Whiston et al. "Expert assessments of the cost and expected future performance of proton exchange membrane fuel cells for vehicles". In: *Proceedings of the National Academy of Sciences* 116.11 (2019), pp. 4899–4904. ISSN: 0027-8424. DOI: 10.1073/pnas.1804221116. eprint: https://www.pnas.org/content/116/11/4899.full.pdf.

[21] Wei You, Kevin J.T. Noonan, and Geoffrey W. Coates. "Alkaline-stable anion exchange membranes: A review of synthetic approaches". In: *Progress in Polymer Science* 100 (2020), p. 101177. ISSN: 0079-6700. DOI: https://doi.org/10.1016/j.progpolymsci.2019.101177.

[22] Noga Ziv, William E. Mustain, and Dario R. Dekel. "The Effect of Ambient Carbon Dioxide on Anion-Exchange Membrane Fuel Cells." In: *ChemSusChem* 11.7 (2018), p. 1136. ISSN: 18645631.

A Appendix 1: Alkaline stability

^{1}H NMR spectrum from alkaline stability tests.

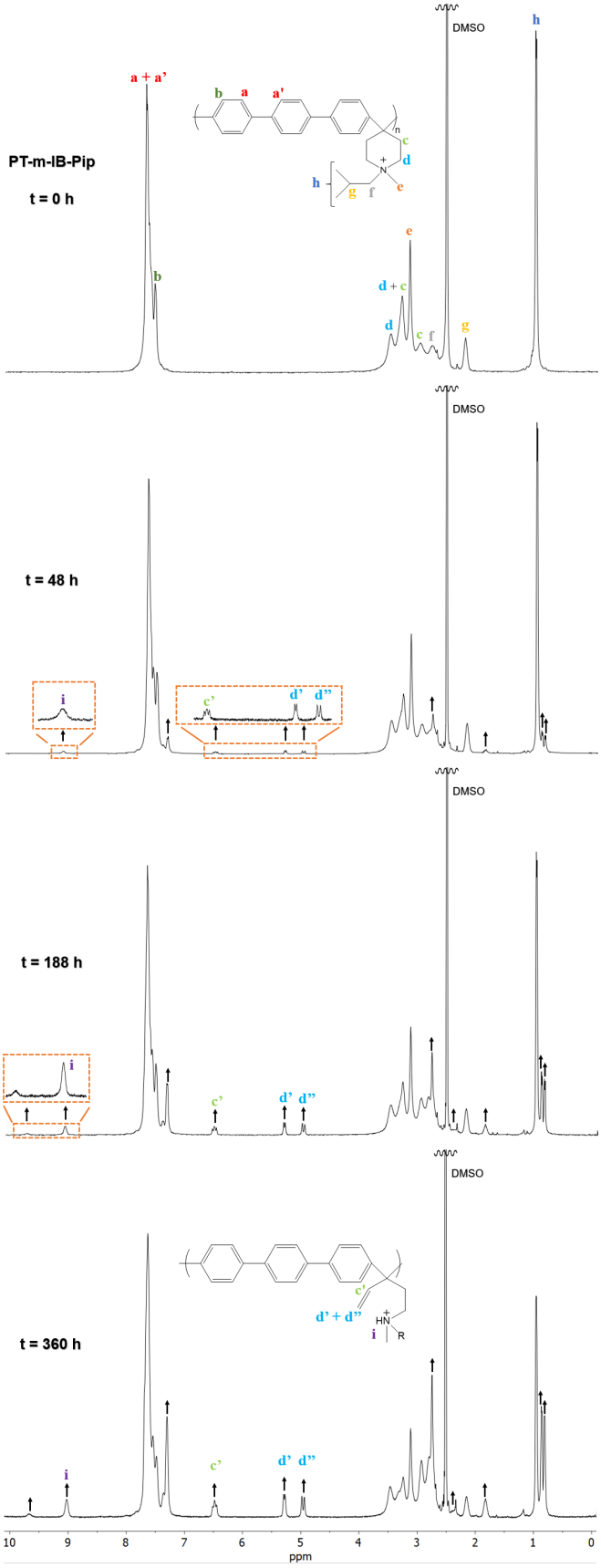

Figure A.1 – ^{1}H NMR spectra of PT-m-IB-Pip before and after immersion in 2M NaOH for 48, 188 and 360h

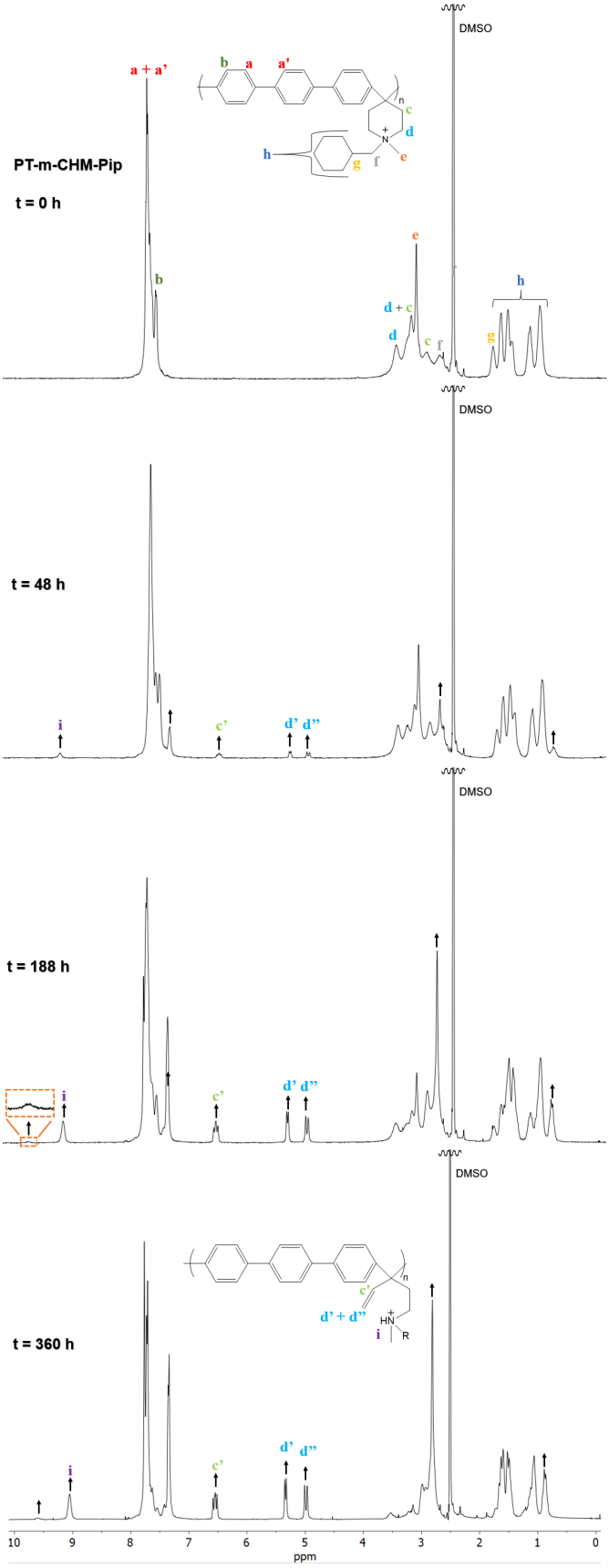

Figure A.2 – ^{1} HNMR spectra of PT-m-CHM-Pip before and after immersion in 2M NaOH for 48, 188 and 360h

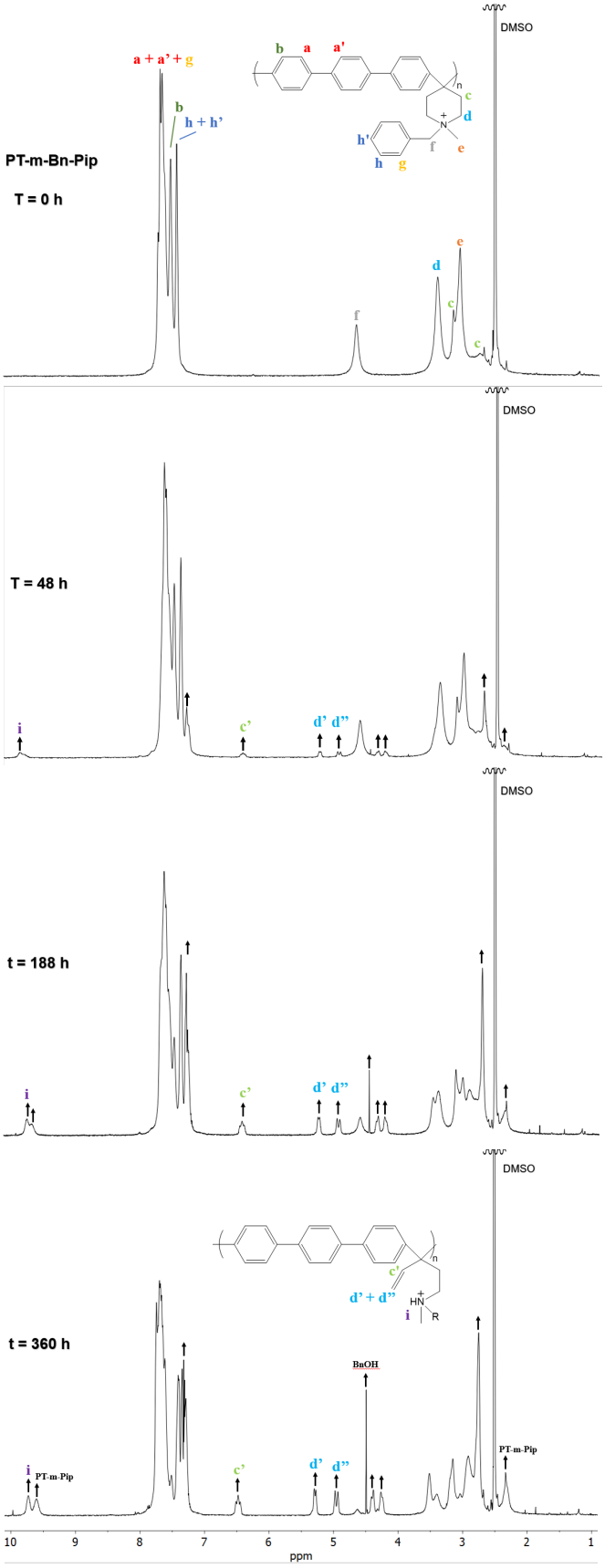

Figure A.3 – ^{1}H NMR spectra of PT-m-Bn-Pip before and after immersion in 2M NaOH for 48, 188 and 360h

B Appendix 2: AEM images

Images of additional AEMs.

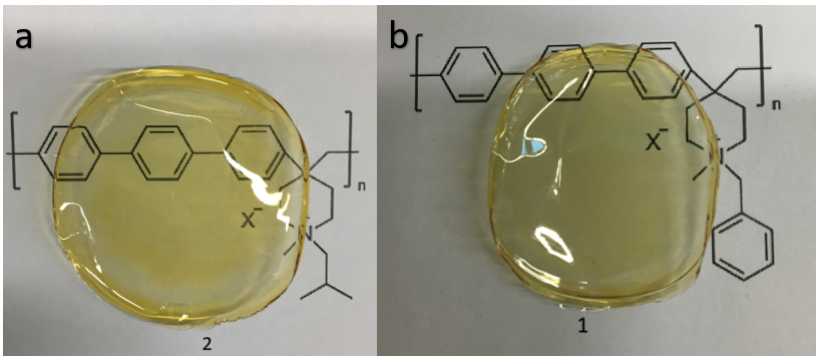

Figure B.1 – Membranes of a: PT-m-IB-Pip and b: PT-m-Be-Pip

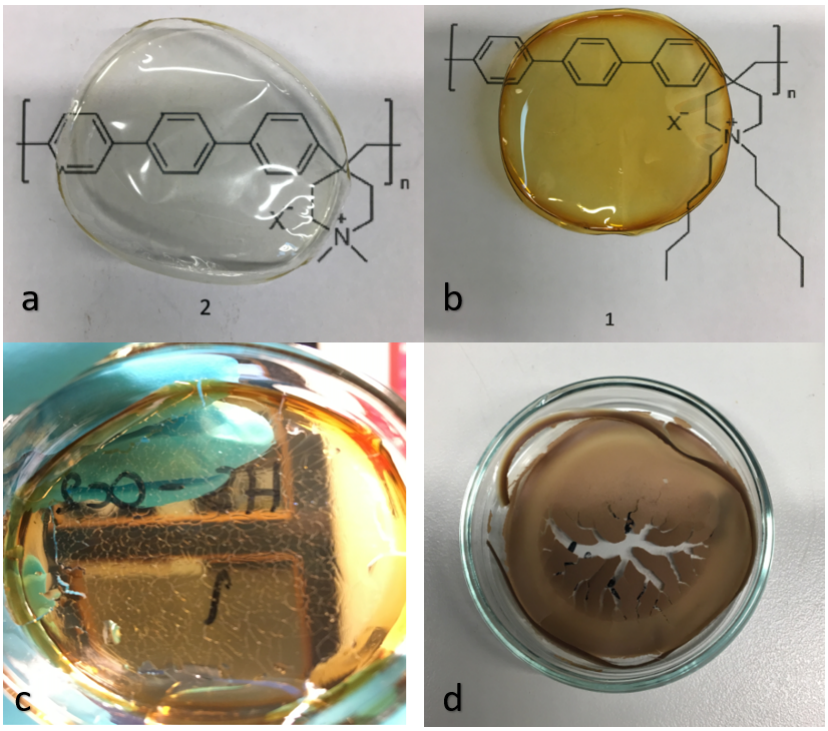

Figure B.2 – Membranes of a: PT-diMe-Pip, b: PT-diHe-Pip, c: PT-diOc-Pip and d: PT-diBu-Pip

C Appendix 3: List of chemicals

p-terphenyl (Sigma Aldrich 99.5%), TFA (Sigma Aldrich, 99%), TFSA (Fluorochem), Iodomethane (Sigma Aldrich, 99%), 1-Bromobutane (Sigma Aldrich, 99%), 1-Bromohexane (Sigma Aldrich, 98%), 1-Bromooctane (Chemicon, 99%), 1-Bromo-2-methylpropane (Sigma Aldrich, 99%), Benzyl bromide (Sigma Aldrich, 99%), (Bromomethyl)cyclohexane (99%), N,N-Diisopropylethylamine (DIPEA, Sigma Aldrich, 99%), K_2CO_3 (Sigma), NMP (99.%), DMSO (99.5%), 2-propanol (IPA, Sigma Aldrich, 99.8%), Diethylether (Sigma Aldrich, 99.8%), Ethanol (Solveco, 99.7%), Ethanol (Solveco, 95%), NaBr (VWR), NaOH (99%, pellets, Sigma), DMSO-d_6 (99.96 at% D), $NaNO_3$
(Merck), K_2CrO_4 (Fluka Analytical) 4-piperidone monohydrate hydrochloride (Sigma Aldrich 98%) Dichloromethane (unknown)

4-piperidone monohydrate hydrochloride was washed with EtOH and dried under vacuum at RT before use. DCM was dried using an MBraun dry solvent dispenser system MB-SPS 800.